THE REQUIREMENT AND FORMULATION OF A GIC-INCLUSIVE STATE ESTIMATOR FOR GEOMAGNETIC DISTURBANCE EVENTS

A Thesis

by

GANDHALI PRAKASH JUVEKAR

Submitted to the Office of Graduate and Professional Studies of
Texas A&M University
in partial fulfillment of the requirements for the degree of

MASTER OF SCIENCE

Chair of Committee,	Katherine Davis
Committee Members,	Thomas Overbye
	Aniruddha Datta
	Behbood Zoghi
Head of Department,	Miroslav Begovic

May 2019

Major Subject: Electrical Engineering

ABSTRACT

It is widely known that solar Coronal Mass Ejections (CMEs) emanating from the sun's surface have the capacity to disturb the earth's magnetic field. This leads to an event called a Geomagnetic Disturbance (GMD). The varying magnetic field caused due to this disturbance could result in an electric field over the earth's surface. This electric field has the potential to eventually cause quasi-dc currents called Geomagnetically Induced Currents (GICs) circulating through the grid. When these quasi-dc currents flow through high-voltage transformers, they produce additional reactive power losses in them.

Myriad of research efforts have been taken to address the issue of circulating GICs from different perspectives. Improved GIC modelling, electric field estimation, GIC monitoring, stability analysis, and voltage study to list a few. But, none of the efforts have addressed the GMD problem from a Power System State Estimator (PSSE) perspective. PSSE is a tool employed by utilities in Energy Management Systems (EMS) and hence,is an important tool for making decisions pertaining to the grid. The additional reactive losses caused by GICs, being unaccounted for, could result in large deviations in the system states estimated. Therefore, my research is motivated by the lack of an accurate PSSE available for the utilities to be used during GMD events. A GIC-inclusive PSSE could greatly assist the utilities and system operators in taking operational decisions and hence, help in better management of the grid.

The power grid is modelled as a dc system for GIC analysis and study. This is because GICs are quasi-dc and hence the system can be modelled as dc. Various studies that need to be carried out for GMD analysis require computation of transformer neutral GICs as well as other system parameters. A considerable portion of these studies are usually performed on MATLAB®. But, there is no tool or package available on MATLAB that can provide easy and seamless calculations of these necessary parameters. One direct example, relevant to my thesis, of an application of such a tool, would be in the modified PSSE itself. The modified PSSE would require the calculation of transformer neutral GICs. Therefore, another research motivation is the construction of an efficient

tool for the calculation of such system values that could be utilized for various GMD studies.

For my research, the accuracy of the traditional state estimator was checked for GMD events. This state estimator failed to produce accurate results during the GMD events and accumulated noticeable results. To solve this problem, the GIC-Inclusive state estimator was constructed using the GMD tool, MATGMD. This modified state estimator was successful in obtaining accurate results for the EPRI 20 bus case and the UIUC bus case with the error in the voltage magnitude states in the range of 10^{-5} and for the neutral current states in the range of 10^{-4}. The results for the EPRI 20 bus case using the GIC-Inclusive state estimator have been depicted and comparisons with the traditional state estimator have been made. The GIC-Inclusive state estimator, though computationally heavy, is very effective and the advantages of its applications outweighs the ease of using the traditional state estimator during GMD events.

ACKNOWLEDGMENTS

I would like to take this opportunity to thank everyone who I collaborated with and who mentored me throughout my Master's studies. Firstly, I would like to thank my advisor, Dr. Davis, for her continual support and guidance throughout my research. I learned a lot from her and she inspires me not only because of her academic successes, but also because of her enthusiasm and dedication towards her goals. Secondly, I want to thank the committee members for their interest and support for my work. Additionally, I would like to thank Cecilia Klauber for her guidance, patience and encouragement for my work as well as for the direct involvement in the work done in Chapters 3 and 5.

There have been a few more people, who supported and guided me whenever I needed help. I would like to think Komal Shetye, Hao Huang and the GMD project team at the ECEN department at Texas A&M. I would also like to acknowledge my funding sources, the Texas A&M Engineering Experiment Station (TEES) and the National Science Foundation (NSF).

I would like to thank my close friends - Sai Krishna, Meghana and Santosh, for helping me stay focused and for everything I have learned from them. Lastly, I want to thank my family, for their unwavering love, support and sacrifice. They inspired me to achieve what I want. I am and will be forever grateful to them for everything they have done.

CONTRIBUTORS AND FUNDING SOURCES

Contributors

This work was supported by a thesis committee consisting of Professor Davis, Professor Overbye and Professor Datta of the Department of Electrical and Computer Engineering and Professor Zoghi of the Department of Engineering Technology and Industrial Distribution.

The work done in Chapter 3 was a collaborative effort with graduate student Cecilia Klauber. The data used and/or analysed in Chapters 3, 4 and 5 was obtained from PowerWorld®. The development of the code pertaining to the research used MATPOWER as its base.

This thesis is based on two papers I have written, with technical guidance from my fellow co-authors, during my Master's program:

1. C. Klauber, G. P. Juvekar, K. Davis, T. Overbye, and K. Shetye, "The Potential for a GIC-Inclusive State Estimator," in North American Power Symposium (NAPS), 2018. IEEE, 2018, pp. 1-6.

2. G. P. Juvekar and K. Davis, "MATGMD: A tool for Enabling GMD Studies in MATLAB," in Texas Power and Energy Conference (TPEC), 2019. IEEE, 2019, pp. 1-6.

Funding Sources

Funding for my research was provided by the National Science Foundation (NSF) under the award number NSF 15-20864.

TABLE OF CONTENTS

Page

LIST OF FIGURES

FIGURE Page

1. INTRODUCTION

1 Background

The power grid is a critical infrastructure necessary for the unperturbed day-to-day proceedings in the modern society. The power grid today is highly resilient and for the most part manages to reliably and securely deliver power to its customers. But the grid faces challenges that result in disturbances which can be localized or regional and can occur due to both man-made and natural forces. One such natural force that could catastrophically impact a large area is Geomagnetic Disturbance (GMD) which is classified under High Impact Low Frequency (HILF) events. Charged particles from the Coronal Mass Ejections (CMEs) emanating from the sun's surface reach the earth and interact with its magnetosphere-ionosphere. This interaction produces ionospheric currents called electrojets which disturb earth's magnetic field causing a GMD [9, 10]. This can result in rapid change in earth's magnetic field which follows Faraday's Law of electromagnetic induction and causes an electric field over earth's surface. This induces a voltage potential hence resulting in the flow of quasi-dc Geomagnetically Induced Currents (GICs).

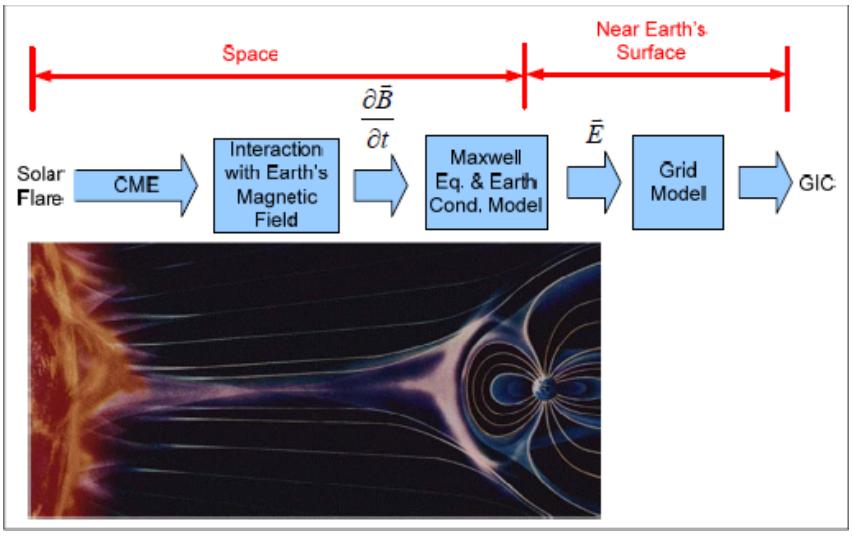

Figure 1.1: Storm interaction with Earth and transmission lines. [1]

As indicated in Fig. 1.1 above, GMD can GICs. This can result in:

- transformer damage due to reactive power losses - caused by half cycle saturation in the transformers due to the presence of quasi-dc GICs,
- loss of reactive power support due to harmonics - could perturb the voltage profile in a localized part of the region or even the entire region that could lead to voltage collapse.

This directly impacts the grid since, firstly, high voltage transformers are crucial for wide-area transmission and secondly, voltage levels need to be within limits for reliable operation. One of the most notable events caused due to GMD occurred in the March of 1989. A blackout lasting nine hours throughout the Hydro-Quebec system was caused because of the cascading transformer failures and a consequent voltage collapse [11]. A large storm hence has the potential to cause catastrophic damage to the grid. The hazard of GMD can leave people without power for long periods of time and can negatively impact important aspects like emergency services and public safety.

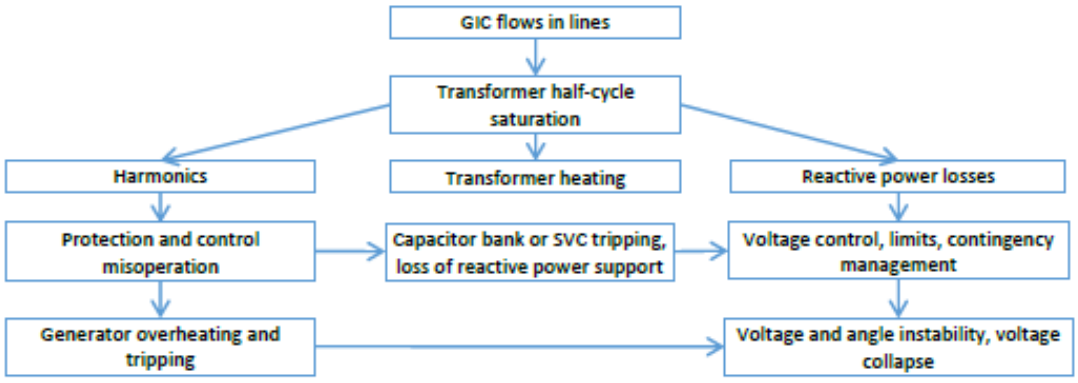

Figure 1.2: The effects of GICs on the grid. [1]

The flowchart in fig.1.2 describes comprehensively, the impact of GICs of the system. The primary effect is the transformer half cycle saturation that could result is three conditions: transformer heating, harmonics and reactive power losses. Harmonics can cause the protection and control devices to mis-operate that could lead to generating tripping and loss of reactive power support. This puts the system in a 'catch22' situation where, the additional reactive power losses in the transformer cause a dip in the nearby bus voltages and are in dire need of reactive power supply. But, the system, with circulating harmonics fail to supply this reactive power due to the

tripping of its reactive power support. Thus, the problem of GMD is compound and focusing on its impact on the Bulk Power System (BPS) is imperative.

This is a multidisciplinary problem beginning at the space weather sciences, and finally reaching the power grid; therefore, involving power system studies. The need for a reliably operating grid is of utmost importance and the industry needs to be equipped to combat the impact of GMD on the grid. This makes reliable monitoring, real-time GMD event analysis and adequate response action plans for the industry crucial. Finding solutions that address these critical aspects is the motivation behind the research carried out from the power system perspective for GMD. Maintaining reliability during GMD, mitigating the effects of GMD and creating awareness prior to an event by estimating its effects are few ways to go about it.

2 Objective

The impacts of GICs have been long known, but as recent as 2014, NERC mandated assessments and plans for the industry to address these impacts [12, 13]. Multitude of research efforts have been taken in the direction of improved GIC modeling, mitigation techniques, reliability assessment, voltage analysis and GIC monitoring to list a few [14–21]. A promising, but not so deeply explored perspective to look at the GMD challenge is from the Power System State Estimation (PSSE) aspect. The overall goal of PSSE is to come up with a power flow model for the present "state" of the power system based on actual measurements[1]. In basic terms, the reactive power loss in the transformers due to GICs during a GMD event needs to be accounted for and a GIC-inclusive or modified PSSE aims to do just that and serve its usual purpose for the industry. This will help the industry incredibly in critical decision making before or during the occurrence of a GMD event and can potentially avoid a catastrophic event from occurring. For a continual operation of the grid even during such events, a modified state estimator can play an essential part in helping the operators take preventive or mitigation action and save the grid from mis-operation.

For my research, I decided move in the direction of the above-mentioned perspective of an ac GIC-inclusive state estimator for the GMD events. An actual formulation of the estimator would

[1] ECEN615 Fall 2018-Lecture 18 by Prof. Thomas Overbye. [22]

require the calculation of certain dc parameters pertaining to GMD events like the GICs. A tool for calculating these parameters is necessary and hence, one of the intermediary goal of my research was to also develop a tool on MATLAB that not only helps in calculating these parameters, but also, could be used for other GMD related studies that focus on reliability, mitigation, modeling, etc. After the tool was developed, it was used in the formulation of the modified state estimator in MATLAB for GMD. The ultimate goal here is to construct an sc estimator that can be used with a good level of surety in the industry for state estimation.

2. LITERATURE REVIEW

1 Background

The first stage of this research process was to review all the existing work on GMD studies from space weather to power systems. This is done in an effort to collect and assimilate existing knowledge, technical know-how and guide the research in a direction leading to beneficial outcomes that aid industry in efficiently managing GMD events on a real-time basis. An in-depth knowledge of the problems helped indicate the immediate challenges that needed to be addressed.

The GMD problem is currently at the last phase where the focus is mainly on analyzing, estimating and modeling the impact on the power grid. This is done using studies, results and data available from the other disciplines that have extensively worked on GMD. This includes disciplines like space weather and geosciences. Hence, the efforts were directed towards tying all the information together with relevant studies and supporting results.

2 Previous Work

2.1 Geomagnetically Induced Currents (GICs) Studies:

Though the GMD event of 1989 at Quebec, Canada was not the most intense event that occurred in history [23], its occurrence had the most catastrophic impact on the grid which consequently had further undesirable effects [24]. GMD, from then on, became a force to reckon with making it a very important topic to be studied in the realm of power systems.

2.1.1 Varying Magnetic Field

As mentioned before, occasionally solar flares originating from the sun's surface reach Earth travelling at high speeds [10] which upset Earth's magnetic balance, causing intense magnetic field variations. During normal conditions, the Earth's magnetic field is usually between 25000 - 60000 nT [25]. The strength of GMDs depends on a variety of factors such as the 11-year sunspot cycle, episodic coronal mass ejection patterns, and seasonal magnetic field coupling that are capable of

combining constructively [26]. The magnitude of variation in the magnetic field at a location can be indicated using the Kp-index that could range from 1-9 depending on the nT variation in the horizontal direction over a period of 3 hours [23]. K and A_p indices are other two parameters that are used for magnetic field variation intensity [1].

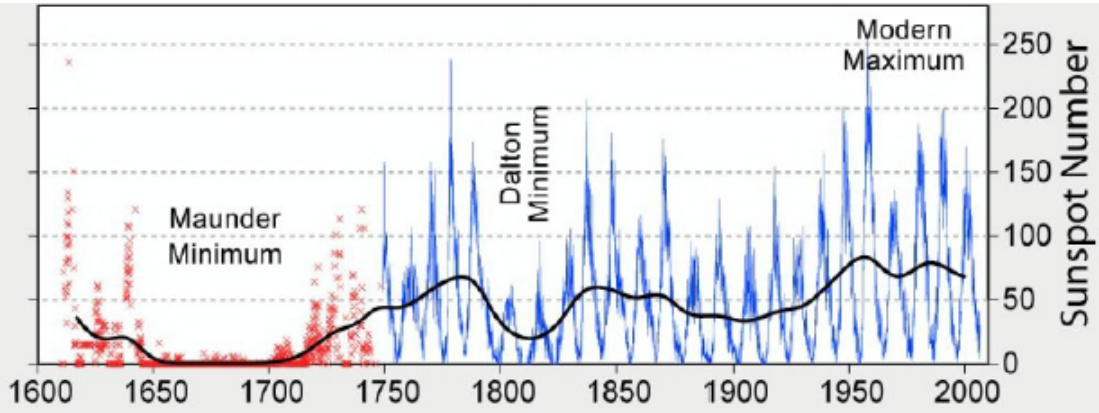

Figure 2.1: 400 years of sunspot observations. [2]

2.1.2 Discussion on the Induced Electric Field

The variation in the Earth's magnetic field causes an electric field on Earth's surface according Maxwell-Faraday's law of electromagnetic induction. This electric field depends on the deep earth conductivity [28,29]. There are two models available to represent the conductivity - the commonly used 1-D model and the more complex 3-D model.

The electric fields have the potential to penetrate deep into the earth, according to the 1-D model assumptions, and depend on the skin depth that ranges from a few kilometers to 100's of km [30]. Variation in the earth's resistivity needs to be known for the 1-D model. The Fig. 2.2 shows the 1-D layered earth model.

The earth is modelled as a series of conductivity layers of varying thickness. The impedance, Z, at a particular frequency is calculated using a recursive approach, starting at the bottom, with each layer having a propagation constant [1]. Using an estimated magnetic field intensity and this earth surface impedance, the electric field can be calculated as follows,

[1] Station K and A indices [27]

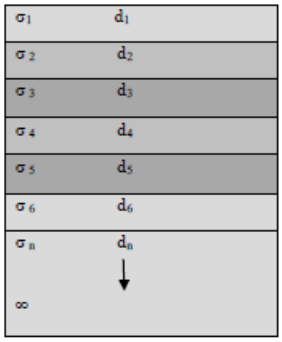

Figure 2.2: The 1-D layered earth conductivity model. [3]

$$E_x(\omega) = Z_{rg}(\omega)H_y(\omega) \tag{2.1}$$

$$E_y(\omega) = -Z_{rg}(\omega)H_x(\omega) \tag{2.2}$$

where, the magnetic field intensity is $H_x(\omega)$ (A/m) in the northern direction, the magnetic field intensity is $H_y(\omega)$ in the east direction, the electric field is $E_x(\omega)$ (V/m) in the north direction, the electric field $E_y(\omega)$ in the east direction, and the earth surface impedance is $Z_{rg}(\omega)$ (Ω) of a region "rg" at a frequency ω.

There is a library consisting magnetotelluric (MT) measurements that have been recorded over a large area of the US [31].The 3-D conductivity model is based on it. Over a period of time, magnetic and electric fields were recorded at each location given in Fig. 2.3. Transfer functions (EMTFs) were obtained by transforming these measurements in the frequency domain. EMTF are publicly available through IRIS [32, 33]. Electric fields at the earth's surface can be extracted from the magnetic field using these EMTFs.

Similar to Eqn 2.1 and Eqn 2.2, the electric field at every EMTF location can be computed as follows,

$$\begin{bmatrix} E_x(\omega) \\ E_y(\omega) \end{bmatrix} = \begin{bmatrix} \xi_{xx}(\omega) & \xi_{xy}(\omega) \\ \xi_{yx}(\omega) & \xi_{yy}(\omega) \end{bmatrix} . \begin{bmatrix} B_x(\omega) \\ B_y(\omega) \end{bmatrix} \tag{2.3}$$

where ξ is the surface impedance and B is the magnetic field.

The discussion on the electric field is of importance because it is the cause for circulating GICs in the system that consequently cause problems. Inaccurate conductivity information can

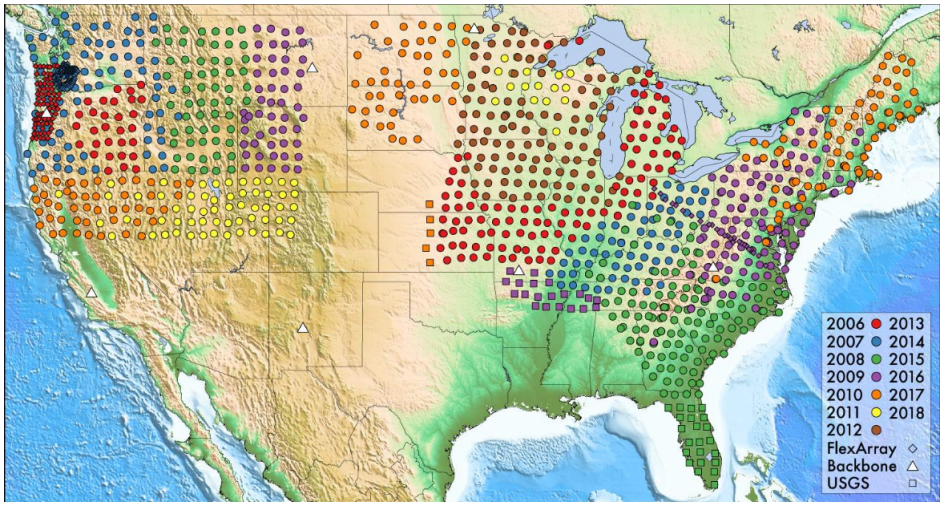

Figure 2.3: Locations in the US where magnetotelluric measurements are obtained [4]

contribute to inaccurate electric field predictions and thus inaccurate GIC predictions [34]. The estimated electric field which is calculated from the magnetic field values measured should approximate the values of GICs well. This is an important research topic which is being currently explored. There have been efforts to estimate the electric field from the GICs measured at transformers using different estimators. The effectiveness and reliability have also been studied for these estimators [14, 15]. The estimated electric field would play an important role in the modified PSSE research since its accuracy along with the granularity/resolution with which it is known directly impacts the GIC calculations. Also, another important discussion would be the relationship between the accuracy of calculated GIC and the granularity/resolution of electric field information available.

2.1.3 GIC Modeling

The magnitude of GICs circulating depend on the magnitude and direction of the electric field along with the topology and dc parameters of the system [35–37]. Since, the geoelectric field can induce quasi-dc voltages in the transmission lines, the GICs are modeled via a dc network analysis [38] given by:

$$\mathbf{I} = \mathbf{GV} \tag{2.4}$$

where G is a conductance matrix (in Siemens) which includes values for substation nodes as well. The vector $\mathbf{V}$ consists the bus dc voltages along with the substation dc voltages. $\mathbf{I}$ is the injection current at every node - bus and substation, which is linearly dependent to the electric field $\mathbf{E}$ as well as the length and direction of the transmission lines. The GIC flowing from a node n to a node m in the network is given by

$$I_{nm} = g_{nm}(V_n - V_m) \tag{2.5}$$

where g_{mn} is the connecting line/transformer conductance.

Let $\mathcal{I}_t$ be the effective per phase current for the transformer t. For delta-wye transformers, $\mathcal{I}_t$ is the current only flowing through high-side winding. For autotransformers and wye-wye transformers, $\mathcal{I}_t$ is a combination of the currents flowing through both high-side and low-side coils. According to [39],

$$\mathcal{I}_t = \mid I_{H,t} + \frac{I_{L,t}}{a_t} \mid \tag{2.6}$$

where $I_{H,t}$ is the per phase GIC flowing through the high side transformer coil, $I_{L,t}$ is the per phase GIC flowing through the low side transformer coil, and a_t indicates the transformer turns ratio.

2.1.4 Reactive Power Losses in Transformers

As seen previously, GICs flowing through the system transformers cause half cycle saturation in these transformer cores. The dc GICs superimpose themselves on the normal ac current flowing through the transformer. This superimposition leads to core saturation during one-half on the cycle and results in high magnetizing currents. Due to these higher magnetising currents, the effective reactive power that is absorbed by the transformer increases. Hence, GICs flowing in the system result in additional reactive power losses which are significant for high voltage, high power transformers.

These losses depend linearly on the effective GICs of the transformer. The reactive power loss in a transformer can be computed using:

$$Q_{loss,t} = k_t V_{pu,t} \mathcal{I}_t \tag{2.7}$$

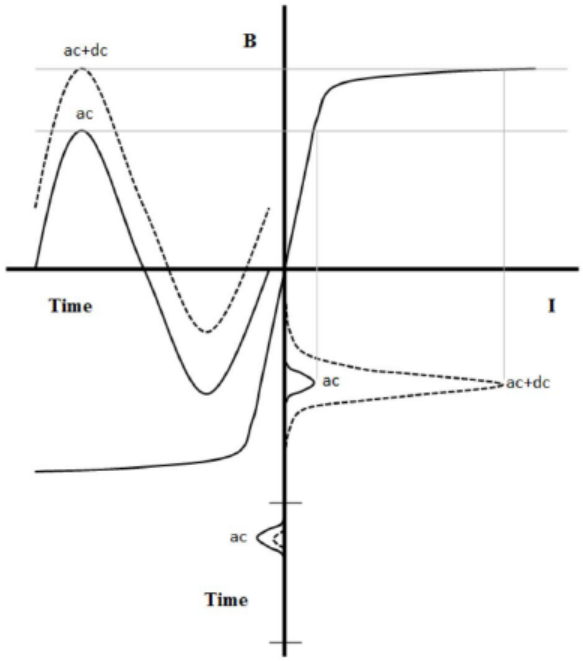

Figure 2.4: Half cycle saturation of transformer core due to GICs [5].

where $V_{pu,t}$ is the ac voltage in per unit at the high side bus of the transformer t, and k_t (Mvars/amp) is a scalar dependent on the transformer [40]. Though the GIC is a dc value, the reactive power loss is an ac phenomenon. The system equations need to account for this reactive power loss and hence, modifications in the system model are necessary for ac analysis.

2.2 Traditional Power System State Estimation (PSSE) Studies

Real-time monitoring of the system in question is possible, using measurements obtained from Supervisory Control and Data Acquisition (SCADA) or increasingly Phasor Measurement Units (PMU) data, because of state estimation. Security and control of the system is crucial and the knowledge about the states provides situational awareness for enabling management of the system [41, 42]. For an ac power system, PSSE is formulated as an over-determined system. It consists of nonlinear equations which can be solved using the Weighted Least Square (WLS) method [42]. Let $\mathbf{x}$ comprise of the states of the system, the length of this vector is n and $\mathbf{z}$ comprises of the measurements obtained from measurement devices, the length of this vector is m, The model relating the states to the measurement is given by:

$$z_i = h_i(\mathbf{x}) + \mathbf{e_i} \tag{2.8}$$

which is non-linear. From the above equation, $h_i(\cdot)$ can be thought of as the non-linear function that relates the states $\mathbf{x}$ to each measurement z_i. The measurement error, e_i is assumed to have a zero mean and variance σ_i^2. For a power system state estimator, the states, $\mathbf{x}$, are mostly bus voltage angles and magnitudes in that order. The measurements, $\mathbf{z}$, comprise of real and reactive power flows and injections, the angle differences, voltage magnitudes, and current flows and injections, turns ratios and phase shift angles (for transformers) if available. The optimization problem of weighted least square estimation has a quadratic objective that needs to be minimized and the power flow equations are the equality/inequality constraints.

$$\mathbf{J}(\mathbf{x}) = \frac{1}{2}\sum_{i=1}^{n}\frac{r_i^2}{\sigma_i^2} \tag{2.9}$$

By formulating it as an unconstrained optimization problem, iterative methods are used. Here, r_i is $z_i - h_i(\mathbf{x})$ which is the residual. The Jacobian matrix $\mathbf{H}$, the measurement variance matrix $\mathbf{R}$, and the residual $\mathbf{r}$ are related using the first-order optimality condition. Using the Taylor series expansion, but ignoring smaller, second-order terms, we get:

$$\mathbf{G}(\mathbf{x}^k)\Delta\mathbf{x}^k = \mathbf{H}^T(\mathbf{x}^k)\mathbf{R}^{-1}\mathbf{r}(\mathbf{x})$$

$$\mathbf{x}^{k+1} = \mathbf{x}^k + \Delta\mathbf{x}^k$$

Here, the Gauss Newton method is used to compute the states. The gain matrix is given by: $\mathbf{G} = \mathbf{H}^T\mathbf{R}^{-1}\mathbf{H}$.

Ill-conditioning and convergence are issues that need to be dealt with which occur because of either varying or inaccurate weighting factors. Errors due to topology and parameter can also arise if care is not taken while modeling the system. There have been efforts to improve the numerical robustness of practical solutions [43].

3. THE POTENTIAL TO EMPLOY A GIC-INCLUSIVE STATE ESTIMATOR*

1 Motivation

A highly deployed tool for grid monitoring in real-time and consequent analysis is Power System State Estimation. With information about the "state" of the system through voltage data, both angle and magnitude, the operators can make decisions pertaining to grid control and security. The traditional states obtained are mostly ac per unit (pu) voltage magnitude and angle at all the buses in the system under study. The utilities or regulating authorities use the state estimator at short intervals (1 - 5 mins) [44]. The solution for the states extracted from the estimator is used as a starting point for many other subsequent applications. For example, the Energy Management System (EMS) at ERCOT uses state estimation as a precursor to the the Real Time Contingency Analysis (RTCA), Voltage Support Service (VSS) and other complex network tools [45]. As these crucial applications evaluate the security and reliability of the system, the accuracy of the state estimator run is of utmost importance.

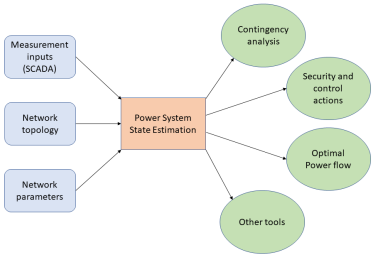

(a) State Estimation flow chart

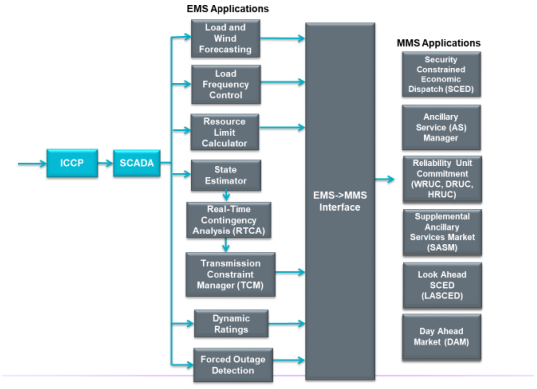

(b) ERCOT EMS example [1]

Figure 3.1: State Estimation visualised.

*Reprinted with permission from IEEE from - C. Klauber, G. P. Juvekar, K. Davis, T. Overbye, and K. Shetye, "The Potential for a GIC-Inclusive State Estimator," in North American Power Symposium (NAPS), 2018. IEEE,2018, pp. 1-6

[1]ECEN615 Fall 2018-Lecture 19 by Prof. Thomas Overbye. [46]

From the last chapter, it is apparent that GMD events have the potential to cause an increase in the reactive power losses in the transformers. The increased absorption can lead to dipped voltage at some of the buses around the transformers affected gravely. The harmonics in the system that trip the reactive power support, leading to an unattended low voltage event. An operator looking at the state estimator results will receive imprecise information about this voltage. These errors in modelling maybe attributed to topology errors or even bad data skew. The operator may not realise the preventive actions that are needed to be to taken to assuage the situation from worsening. The situation, if not heeded, can lead to voltage instability issues eventually causing a total voltage collapse.

Be it a local event of loss of power or a total system collapse, it is not desired. The system would have to be energised from a possible blackout and procedures required to blackstart the system would have to be followed. This is a time-consuming as well as an arduous process requiring steps to be followed carefully. Not to mention the problems faced by the consumers due to loss of power. Hence, a GMD event occurrence requires precise monitoring that can be facilitated by the use of a modified state estimator that is GIC-inclusive.

This section of my thesis is based on a paper I worked on [7]. As mentioned earlier, the state estimation approach has not been worked on before to the best of my knowledge. With the UIUC 150 bus case [6, 47], the performance of the traditional state estimator was analyzed and the motivation to change the model by incorporating additional reactive power is discussed with a few model recommendations.

2 Testing the case and Results

2.1 UIUC 150 bus case

Depicted in fig. 3.2 below is the 500/230 kV, UIUC 150 bus synthetic system [6] which is the test case for the state estimation study here. This system is tested for various GMD scenarios of varying magnitudes and varying directions of electric field using the PowerWorld simulator. For the different electric field scenarios, the GIC flow is solved using the system dc parameters and the

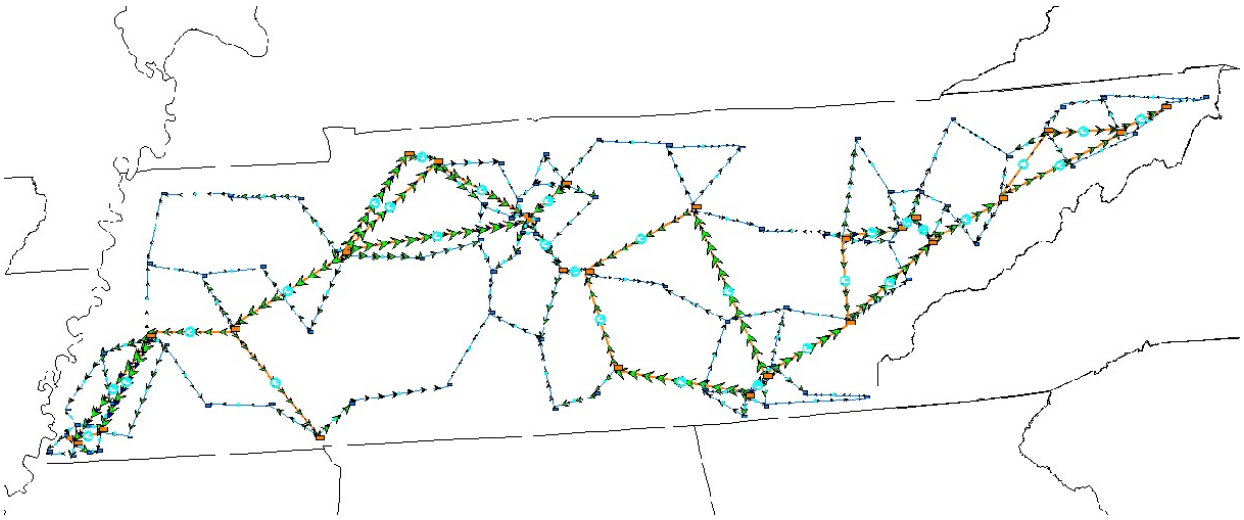

Figure 3.2: One line diagram for the UIUC 150 bus system (synthetic). [6]

reactive power losses are calculated for the saturated transformers in the system. On the ac side, the power flow is solved with these reactive power losses are accounted. The perfect measurements are obtained from the simulator to be used for the state estimator. To generate noisy measurements, random Gaussian noise is added to these perfect measurements exported using MATLAB. The noise level for voltage magnitude measurements used is $\sigma_i = 0.01$ and for power flow and injection measurements is $\sigma_i = 0.02$.

The measurements available to the state estimator as the input set are randomized. This is because, in reality, the number of buses and lines monitored are limited. What this means is, we do not have information for each bus or line. The algorithm was constructed to include results only for the cases which were observable - measurements that included well distributed measurements with adequate coverage. For the power flow measurements, the percentage of maximum measurements given as input range from 55%-80%. For the power injection measurements, the percentage of maximum measurements given as input range from 65%-100%. For the voltage magnitude measurements, the percentage of maximum measurements given as input are up to 50%.

2.2 Results

The surface electric field induced by varying magnetic field could have varying directions as well as magnitudes. For the description and illustration of the inadequacy in the estimation of the system states during a GMD event, the use of uniform electric field scenarios is sufficient.

For the first study, the direction of the electric field is kept fixed at 50° and the magnitude of the electric field is increased from 1 V/km to 9 V/km in steps of 1 V/km. The fig. 3.3 illustrates the relationship between the average absolute error and storm magnitude.

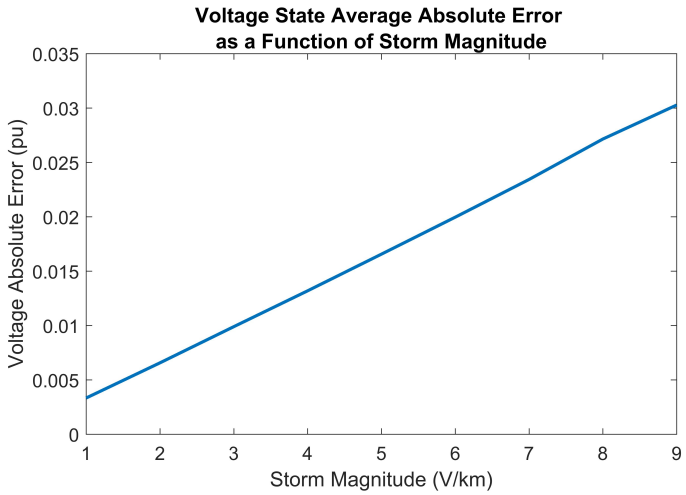

Figure 3.3: Increasing average absolute voltage error with increasing storm magnitude. Reprinted from - [7]

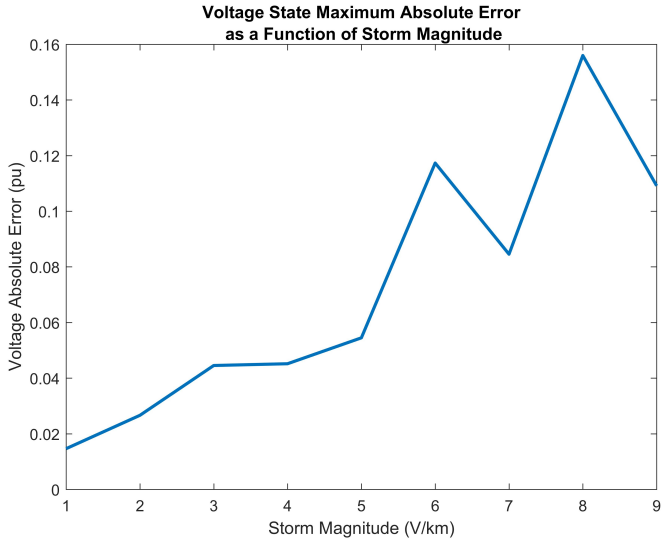

Figure 3.4: Increasing maximum absolute voltage error with increasing storm magnitude. Reprinted from - [7]

Here, the error is averaged over 100 simulations for all the system states. It is the difference between the estimate and the actual voltage magnitude. The fig. 3.4 illustrates the relationship between the maximum absolute error and storm magnitude. The increase in the error can be ascribed to the increase in the reactive power losses as the magnitude of storm increases.

For the second study, the magnitude of the electric field is kept fixed at 4 V/km and the direction (angle) of the electric field is increased from 0 to 360° in steps of 20°. There is a cyclical pattern or trend observed in the error as shown in fig. 3.5. This can be attributed to the fact that GICs of higher magnitude will be induced on lines which are parallel to the direction of storm causing increased reactive power losses as they flow to the ground through the transformers in the system.

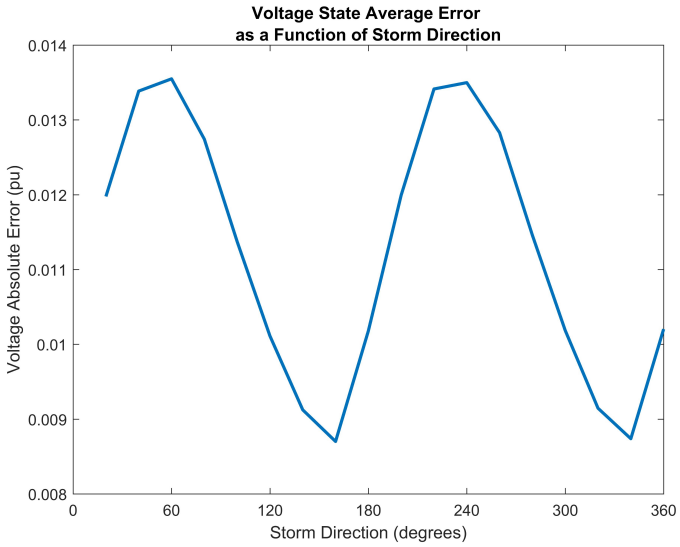

Figure 3.5: By varying the direction of the storm from 0 to 360°, there is a periodic pattern observed in the the average absolute voltage error. Reprinted from - [7]

For the last study, the storm direction and magnitude are kept fixed at 50° and 4 V/km respectively. The total number of measurements were kept constant and the percentage of power flow and power injection measurements were varied. From fig. 3.6, it is apparent that as the percentage of measurements that belong to power flow increase (hence, the measurements that are power injections decrease), the average absolute error in the voltage magnitude state decreases. The reason can be explained as follows: A measurement of the reactive power injection at a bus is actually a summation of all reactive power flows at that bus. This includes the transformer branches which

experience additional reactive power losses during a GMD event. These injections are not modeled correctly in the state estimator and hence, increasing the number of injections increases the possibility of including these incorrectly modeled bus injections. Therefore, as compared to an increase in the flow measurements, the error will be higher for increase in injection measurements. On the other hand, one or more noisy power flow measurements has the capability to increase the error in the voltage magnitude state as seen from fig. 3.7. This occurs because of a strong coupling between voltage magnitude state and the reactive power flow measurement.

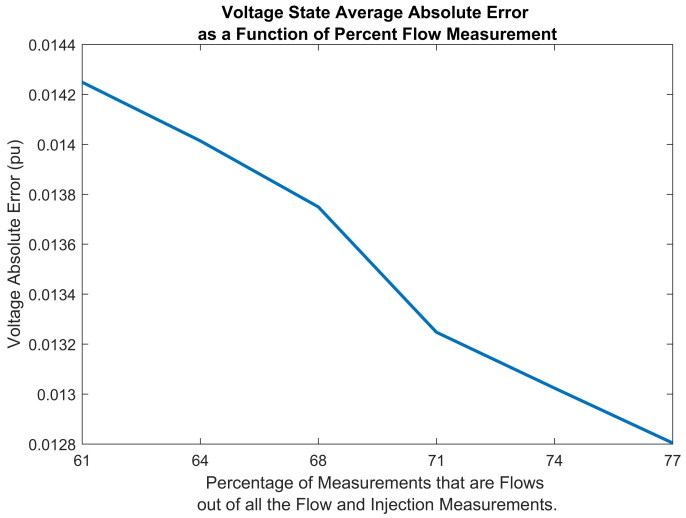

Figure 3.6: The relationship between the average absolute voltage error and the percentage of power flow measurements. Reprinted from - [7]

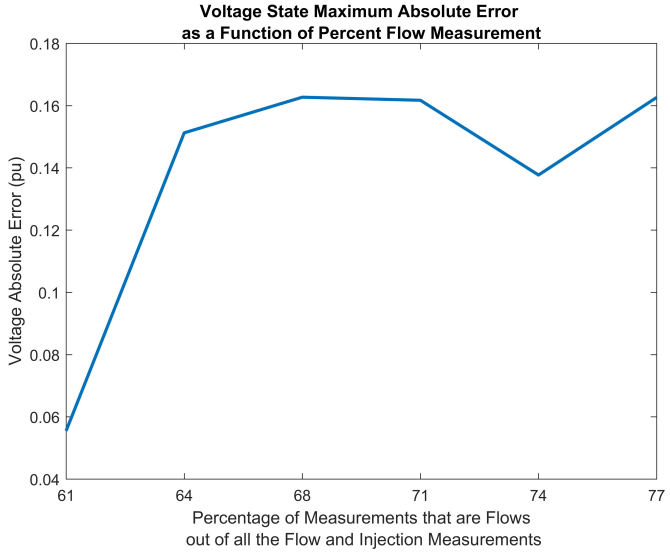

Figure 3.7: The relationship between the maximum absolute voltage error and the percentage of power flow measurements. Reprinted from - [7]

3 Recommendations

From the previous section, it is obvious that the state estimator model that does not account for the effects of GICs (reactive power losses in the transformers) causes error in the state estimates. These errors can further disseminate through applications that use the state estimates as the starting point. The inclusion of the GIC effects in the model for state estimation is not an task. Limitations in the modeling as well as metrology could impede the functional implementation and progress of such programs. The probable issues are described in the this section and recommendations are proposed to facilitate the practical integration of the effects of GICs in the GIC-inclusive state estimator model.

3.1 Network Model Considerations

For the GIC analysis, it is important to have information about the dc system parameters which are generally not required for the conventional power flow analysis. For example, transformer parameters like the dc winding resistances (required for the building of the $\mathbf{G}$ matrix needed to find $\mathbf{V}$ in Eq. 2.4) and the scalar parameter, k. According to 2.7, the effective GIC reactive losses are related to effective GIC current for a transformer through the k parameter value. For precise GIC analysis computations and subsequent state estimation results, the accurate values of these system dc parameters is necessary.

Another important parameter required, that needs to be taken a look at, is the substation grounding resistance. Even though the value of this parameter can be measured on field, it is highly dependent on the conditions of the soil. It is also controlled by the atmospheric conditions that vary - temperature being one. For analysis, there are often attempts to either estimate this parameter value or an outdated measurement is used by the operators. The substation grounding resistance can be estimated using various techniques albeit the requirement of adequate placement of GIC measurements [48]. GIC reactive power losses can be incorporated, using these relationships describing that estimate of the parameter values, into the standard ac state estimator. This state estimator developed would be time-varying which can be utilized for the validation of the substation grounding

resistance values. By principle, as many GIC measurements would be needed as the resistances to be estimated.

3.2 State Estimation Formulation Considerations

The squared form of the gain matrix, $\mathbf{H}^T\mathbf{H}$, can lead to the ill-conditioning issues in the traditional state estimator. There have been various efforts aiming towards improving the convergence characteristics. An obvious way to improve state estimation during GMD events is to account for the GIC effects by including the reactive power losses in the model. Including additional states like GIC neutral currents can help integrating these GIC effects into the estimator model. Traditional state estimation state variables like the voltage magnitude along with the ac system parameters like admittance can help compute all the flows, injections and other system values. Similarly, during GMD events, inclusion of GIC neutral currents, electric field data and/or induced dc node voltages could help get the overall picture of the system. With additional states and their corresponding relationships with the measurements, improving the conditioning of the gain matrix is imperative. Existing techniques used to improve the conditioning number may be relevant but the new states can spring up complicated dependencies and computational efficiency could be at stake.

3.3 Increased Measurement Availability

Getting appropriate measurements for the GIC-inclusive state estimator is a major obstacle. The efforts taken to increase the information availability of the magnetic field have been very fruitful but there are still areas that are not metered adequately in the United States. Another hurdle faced is related to the data regarding conductivity which would also benefit from additional metering. Conductivity information is required to extract the electric field data that is transformed from the magnetic field. There are GIC monitoring devices installed at only a few places in the grid. Also, this data can be highly noisy and hence, not usable all the time. Installation and maintenance of these GIC-measuring devices is expensive but the advantages these devices could provide are innumerable. An accurate (GIC-effects inclusive) system model for state estimation in conjunction with the appropriate measurements facilitated by these monitoring devices could

improve the estimation of the new system states by an extensive amount. This will consequently benefit applications that use (or will use) these states as a starting point. The significant assistance of tools like the GIC-inclusive state estimator should motivate the utilities and operators to improve system infrastructure by investing in appropriate and necessary meters. Specific concerns regarding measurement availability have been outlined in the sections below:

3.3.1 System Observability

For a GIC-inclusive state estimator, where variables such as neutral GIC and/or electric field can get appended to the state vector, the problem of observability can intensify. The inclusion of these states makes it crucial to have sufficient, well-spread measurements across the system under study making state estimation possible. Lack of sufficient and scattered measurements can make the system unobservable. To counter this issue, it is vital to determine the dependencies and relationships that govern observability to ascertain the critical measurements. Typically, the observability analysis utilizes algorithms which are numerical and topological [49, 50]. With the modified state estimator, newer algorithms need to be developed that consider the GIC-related values.

3.3.2 Measurement Redundancy

The ratio of the number of measurements to the number of states is the measurement redundancy. Often, the measurement redundancy is between 1.7-2.2 for practical transmission systems [42] and a lower value for distribution systems. To filter out the noise in the state estimation, higher redundancy is preferred. Diagnosing bad data or topology errors requires additional techniques to be put in place. For the enhancement of measurement redundancy and observability, construction of meter placement algorithms is required.

3.3.3 Unknown Measurement Error Parameters

For a WLS method formulation, the variance σ_i^2 of the measurement error e_i is related to the weightage of that measurement which is a crucial element. For the general power flow, power injection, and voltage magnitude measurements, there is an ballpark understanding of what these

variance values are but for the GIC-related parameters, there is no such standard. If electric field (a logical input for the dc modified state estimator) is a measurement input the state estimator, a significant error would be encountered. This is because the “measurement" would actually be the value extracted by transforming a measurement acquired from a magnetometer (with its own error) via conductivity profiles. This leads to an error that is a result of cascading on various errors throughout the process. Availability of real data as measurements for studies in the future would improve the decisions regarding the error variance to be used for the GIC-related values.

4. MATGMD*

1 Motivation

For my master's research on the ac GIC-inclusive state estimator, I decided to append per-unit (pu) neutral GICs to both, the state vector as well as the measurement vector. The assumption is that the electric field information received is fairly accurate - it could be estimated data extracted from magnetic field data and conductivity profiles or it could be real data. Hence, electric field is not a state or a measurement input for the state estimator. The source of the electric field information is not relevant. The error variance of the electric field data is also not considered. This is because, the electric field data is only used as a starting point.

Similar to the traditional states like voltage magnitude and angle of the traditional state estimator, the additional state of the GIC-inclusive state estimator needs an initial value. For voltage magnitude and angle, the initial values are 1.0 pu and 0° which are suitable starting points for these bus parameters. The pu neutral GIC state also requires an apt starting point through appropriate initial values. These initial values can be obtained by using the electric field data that is assumed to be fairly accurate through a series of equations that relate the electric field to the pu neutral GICs using information like system topology and parameters. The details of the equations will be described in the next section.

Another important computation required for the modified state estimator is the pu effective GICs for calculating the reactive power losses in the transformers during a GMD event. During every iteration of the state estimation, the new, updated pu neutral GIC is obtained which then can be used to compute the effective GIC for further calculations (the reactive power flow and injection estimates as well as for the terms in the Jacobian, $\mathbf{H}$) required during each iteration.

The state estimation studies were being carried out on MATLAB but there was no tool or package available on this platform for computations related to dc GIC modeling that would help

*Reprinted with permission from IEEE from - G. P. Juvekar and K. Davis, "MATGMD: A tool for Enabling GMD Studies in MATLAB,"in Texas Power and Energy Conference (TPEC), 2019. IEEE, 2019, pp. 1-6

in the extraction the neutral GICs and/or effective GICs if electric field data was fed along with the system topology and essential system dc parameters. Hence, a tool/package that enabled these functionalities had to be developed not only for addressing the requirements for the state estimation problem, but also, for various other studies like mitigation techniques and reliability intended to be performed on MATLAB.

2 System Modeling

The system modeling for GMD events causing GICs to flow in the system has been detailed in this section along with the explanation of the development of the package in MATLAB. The tool uses the electric field data as one of the input parameters along with the system topology and dc system parameters. It is equipped with the ability to analyse both uniform and non-uniform electric field. The capability to analyse non-uniform electric field facilitates extensive studies on real-life GMD scenarios that result in non-uniform electric field over the network region. A uniform electric field is represented as $E = [E^N, E^E]^T$, where the north and east directions are denoted by the superscripts N and E, respectively. The non-uniform electric field functionality can be utilized if the electric field data is obtained in a manner similar to b3d files with the longitude and latitude details - the input file for the non-uniform case will be described soon.

2.1 Input file format

Data files in MATLAB are either M-files or MAT-files that define and return output matrices. Any standard text editor can be used to edit the M-file whose format is plain text. For MATGMD-compatible input files, the mandatory output fields for the data files should be

- **Xmr**: transformer dc information,
- **Bus_dc**: bus dc information,
- **Substn**: substation dc information and,
- **Lines**: transmission line dc information,

where all the fields are matrices.

Optionally, **Ckt_n**: circuit numbers for combined transformer and transmission line branches, can be an output field depending on its necessity. The modified state estimation problem requires circuit numbers. For a uniform electric field analysis, **E**: directional magnitudes of the uniform electric field in the north and east direction, is also an output field. For individual matrices, every row describes or details a single transformer branch, bus, substation or line. The number of rows in **Xmr**, **Bus_dc**, **Substn** and **Lines** are given by **n_x, n_b, n_s** and **n_l**, respectively. The function file, **ext2int_dc.m** can be used to renumber the buses in a consecutive manner if the **Bus_dc** matrix indicates that the buses in the system are not numbered consecutively.

2.1.1 Non-Uniform Electric Field Input

GMD analysis using MATGMD for a non-uniform electric field requires the electric field data to be given as an input through an M-file. The output fields for this file should be

- **Ematrix**: electric field matrix with directional magnitudes (north and east directions) of the electric field in zones defined by latitudes and longitudes.
- **del**: the step size for changing the latitudes and longitudes.
- **lmin**: the vector with the minimum value of the latitude and longitude.
- **lmax**: the vector with the maximum value of the latitude and longitude.

2.2 G matrix

Let N^b be the number of buses for a transmission system. These buses do not include the ones which are connected to the generators grounded via the nearest substation. Let N^s be the number of substations in the system considered. Together, the buses and substations form a set of nodes, $N : N^b \cup N^s$. Let the set of branches between the nodes, n and m where, $(n, m) \subseteq N^b \times N^b$, be denoted by $\mathcal{L}$. This includes transmission lines and transformer branches which are the autotransformer series windings. Let the set of transformer windings, which include the high side winding for a delta$-$wye transformer, the common winding for an autotransformer and both the windings for a wye$-$wye transformer, between the bus nodes and substation nodes, n

and m where, $(n, m) \subseteq N^b \times N^s$, be denoted by $\mathcal{XL}$. Together, $\mathcal{L}$ and $\mathcal{XL}$ constitute the edges, ε represented as $(n, m) \subseteq N \times N$. Let the equivalent conductance between nodes n and m for any $(n, m) \in \varepsilon$ be g_{nm} = g_{mn}. Similarly, grounding conductance of the substation neutral can be represented using g_{nn} for $n \in N^s$. The symmetric and real matrix, G which is an $N \times N$ matrix can be constructed using these notations. These conductance quantities account for all the three phases in parallel. The elements of G can be given by:

$$G_{mn} = \begin{cases} -g_{mn}, & \text{if } (n, m) \subseteq \varepsilon \\ \sum_{v \in N_n} g_{nv}, & \text{if } n = m \subseteq N^b \\ g_{nn} + \sum_{v \in N_n} g_{nv}, & \text{if } n = m \subseteq N^s \\ 0, & \text{otherwise} \end{cases} \tag{2.1}$$

The MATLAB function file for the dc conductance matrix is **G_mat.m**. The above responses for each condition are implemented in the code for the function file that gives the output matrix **g**. This matrix is similar to the reactance matrix **Y**, but with substation nodes included and the dc conductance values of the system used.

2.3 Injection currents

The potential induced due to the electric field at every transmission line is a voltage source that can be modeled as:

$$V_{nm} = E^N L^N_{nm} + E^E L^E_{nm} \tag{2.2}$$

where, the dc potential that is induced is V_{nm} (V), the distance for the line between buses n and m in the north and east directions are L^N_{nm} and L^E_{nm} (km), respectively. Using the Norton's equivalent, this induced voltage can be converted to a dc current injection at each node connecting these lines and is given by:

$$I_{nm} = V_{nm}/R_{nm} \tag{2.3}$$

where, the dc injection current to bus n is I_{nm} (Amps) and the dc resistance on the line between buses n and m is R_{nm} (ohms). The equivalent current injection I_{mn} to bus m equals to $-I_{nm}$ (Amps). The summation of all the current injections at bus n is the overall injection current at a bus n given by:

$$I_n = \sum_{(n,m)\in L} I_{nm} = \sum_{(n,m)\in L} \frac{E^N}{R_{nm}} L^N_{nm} + \frac{E^E}{R_{nm}} L^E_{nm} \tag{2.4}$$

The injected current is simply $I_n = 0, \forall n \in N^s$ because the substations are not directly connected by transmission lines. Stacking eqn. 2.4 for all the N nodes:

$$\mathbf{I} := [I_1, ..., I_N]^T \tag{2.5}$$

The MATLAB function file for the computation of the injection currents for a uniform electric field is **InjC.m** and for a non-uniform electric field is **VarEFV.m**. The above described equations are implemented in the code for the function file mentioned. The calculations for the injection currents involve a simple matrix multiplication between the directional electric field values and the directional lengths of the line for a uniform electric field case. There is an elaborate process for the non-uniform electric field case which involves breaking down the lines into various parts corresponding to the electric field zone they fall in. Then, for every part of the line, the directional length is multiplied with the directional electric field and summed to be later divided by the dc resistance of that line. Directional lengths for each line can be computed by using the location coordinates and the distance formula [3]:

$$L^N = (111.113 - 0.56 * cos(2\phi))\Delta lat \tag{2.6}$$

$$L^E = (111.5065 - 0.1872 * cos(2\phi)) * cos(\phi)\Delta long \tag{2.7}$$

where, L^N and L^E are the North and East directional lengths (km). Here, the difference in the latitudinal and longitudinal coordinates of the from and to substations are given by Δlat and $\Delta long$

respectively. The value of ϕ is given as,

$$\phi = \frac{latA + latB}{2}$$

2.4 DC Node Voltages

Calculating the dc node voltages is a vital intermediary step for the computation of the system GICs and related values. Let the dc voltage at any bus or substation n be V_n (Volts). We get $\mathbf{V} := [V_1, V_2, .., V_N]^T$ by concatenating all the nodes. From the dc power flow model, **G** and eqn. 2.5, we get:

$$\mathbf{V} = \mathbf{G^{-1}I} \tag{2.8}$$

The MATLAB function file that implements the equation for the computation of the dc node voltages is **Vdcnodes.m**

2.5 Substation and Transformer GICs

The GIC flowing at every substation n can be obtained by:

$$I_n^s = g_{nn}V_n, \forall n \in N^s \tag{2.9}$$

At the transformer level, the high-side and low-side transformer GICs can be obtained. The current flowing through the wye side of a delta$-$wye transformer, either side for a wye$-$wye transformer or the common winding of an autotransformer, from bus n to substation m via the transformer in-between, is given by:

$$I_{nm}^T = g_{nm}(V_n - V_m), \forall n \in N^b, m \in N^s \tag{2.10}$$

The current flowing through the series winding for an autotransformer is given by:

$$I_{nm}^T = g_{nm}(V_n - V_m), \forall n \in N^b, m \in N^b \tag{2.11}$$

where the high-side bus and the low-side bus are denoted by n and m respectively. The transformer neutral current in the summation of the high side and the low side currents calculated using eqn. 2.10 and 2.11. The neutral current, I_n^T is given by:

$$I_n^T = (I_H + I_L) * 3, \tag{2.12}$$

where, the per phase high-side and the low-side currents for a transformer are I_H and I_L respectively. Additionally, r_h and r_l correspond to the ratios of the high side and the low side currents to the transformer neutral current respectively:

$$r_h = \frac{I_H * 3}{I_n^T}, r_l = \frac{I_L * 3}{I_n^T} \tag{2.13}$$

The MATLAB function file that implements the equations for the computation of various GIC values is **XmrI.m**

2.6 Effective GICs

The additional reactive power loss (Q_{loss}) in a transformer during a GMD are linearly dependent on the value of the effective GIC for the corresponding transformer. These effective GICs depend on the transformer turns ratio, a. Let t be the transformer under consideration. The effective GIC per phase $I_{eff,t}$ for the corresponding transformer is given by:

$$I_{eff,t} =\mid I_{H,t} + \frac{I_{L,t}}{a_t} \mid$$

where, $I_{H,t}$ and $I_{L,t}$ are the transformer high side and low side currents per phase respectively and a_t is the transformer turns ratio. The equation can also be expressed as:

$$I_{eff,t} =\mid I_n^T(r_h + \frac{r_l}{a_t}) \mid \tag{2.14}$$

The MATLAB function file that implements the equation for the computation of effective GIC values is **Igiceff.m**

2.7 Test case file

The outputs of the test files can be customized as per the need of the user. The study that needs to be performed decides the kind of parameters or values that need to be extracted from the tool since various GMD studies target unique system values.

3 Results

The tool/package developed was then used to calculate the pu transformer neutral GICs for two systems: the EPRI 20-bus case and the UIUC 150-bus case. Uniform electric field scenarios of varying magnitude and varying direction as well as non-uniform electric field scenarios were applied to these systems. The input file for each of the cases was constructed according to Section 4.2.1. and the required system information was extracted. The pu transformer neutral GICs obtained using the tool were then compared and verified using the PowerWorld Simulator. The decimal logarithm of absolute error and the percentage error profile was plotted.

The decimal logarithm of absolute error and the percent error is given by is given by,

$$log_{10} \mid I_{n,calculated} - I_{n,PowerWorld} \mid \tag{3.15}$$

$$((I_{n,calculated} - I_{n,PowerWorld})/I_{n,PowerWorld}) * 100 \tag{3.16}$$

3.1 EPRI 20 bus

The tool is used on the 500/345 kV 20-bus system depicted in Fig. 4.3. Many electric field scenarios were applied out of which four have been depicted in the figures below. The scenarios were as follows:

1. Uniform electric field of magnitude 3 V/km at 20°.
2. Uniform electric field of magnitude 4 V/km at 220°.

3. Non uniform electric field - Case 1

Lat	Lon: -87.500	Lon: -87.000	Lon: -86.500	Lon: -86.000	Lon: -85.500	Lon: -85.000	Lon: -84.500	Lon: -84.000	Lon: -83.500	Lon: -83.000	Lon: -82.500	Lon: -82.000	Lon: -81.500	Lon: -81.000
34.500	1.800, 0.400	1.750, 0.400	1.700, 0.400	1.650, 0.400	1.600, 0.400	1.550, 0.400	1.500, 0.400	1.450, 0.400	1.400, 0.400	1.350, 0.400	1.300, 0.400	1.250, 0.400	1.200, 0.400	1.150, 0.400
34.000	1.800, 0.500	1.750, 0.500	1.700, 0.500	1.650, 0.500	1.600, 0.500	1.550, 0.500	1.500, 0.500	1.450, 0.500	1.400, 0.500	1.350, 0.500	1.300, 0.500	1.250, 0.500	1.200, 0.500	1.150, 0.500
33.500	1.800, 0.600	1.750, 0.600	1.700, 0.600	1.650, 0.600	1.600, 0.600	1.550, 0.600	1.500, 0.600	1.450, 0.600	1.400, 0.600	1.350, 0.600	1.300, 0.600	1.250, 0.600	1.200, 0.600	1.150, 0.600
33.000	1.800, 0.700	1.750, 0.700	1.700, 0.700	1.650, 0.700	1.600, 0.700	1.550, 0.700	1.500, 0.700	1.450, 0.700	1.400, 0.700	1.350, 0.700	1.300, 0.700	1.250, 0.700	1.200, 0.700	1.150, 0.700
32.500	1.800, 0.800	1.750, 0.800	1.700, 0.800	1.650, 0.800	1.600, 0.800	1.550, 0.800	1.500, 0.800	1.450, 0.800	1.400, 0.800	1.350, 0.800	1.300, 0.800	1.250, 0.800	1.200, 0.800	1.150, 0.800

Figure 4.1: EPRI 20 - Case 1

4. Non uniform electric field - Case 2

Lat	Lon: -88.000	Lon: -86.000	Lon: -84.000	Lon: -82.000
35.000	0.500, 1.000	0.500, 1.000	1.000, 1.000	1.000, 1.000
34.000	0.500, 1.000	0.500, 1.000	1.000, 1.000	1.000, 1.000
33.000	0.500, 1.000	0.500, 1.000	1.000, 1.000	1.000, 1.000
32.000	0.500, 1.000	0.500, 1.000	1.000, 1.000	1.000, 1.000

Figure 4.2: EPRI 20 - Case 2

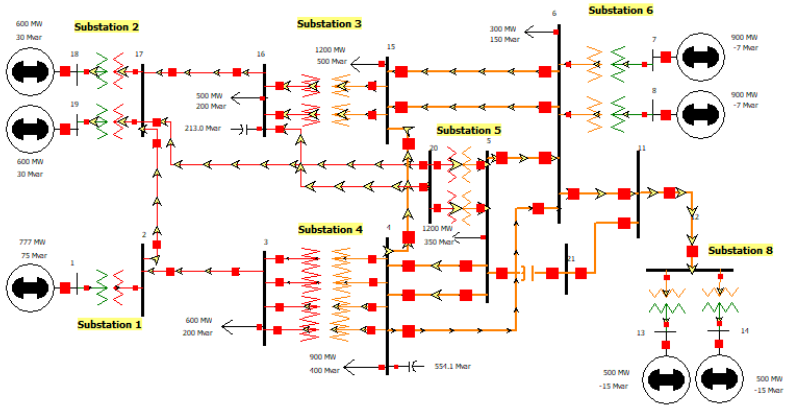

Figure 4.3: One-line diagram of the EPRI 20-bus system [8]

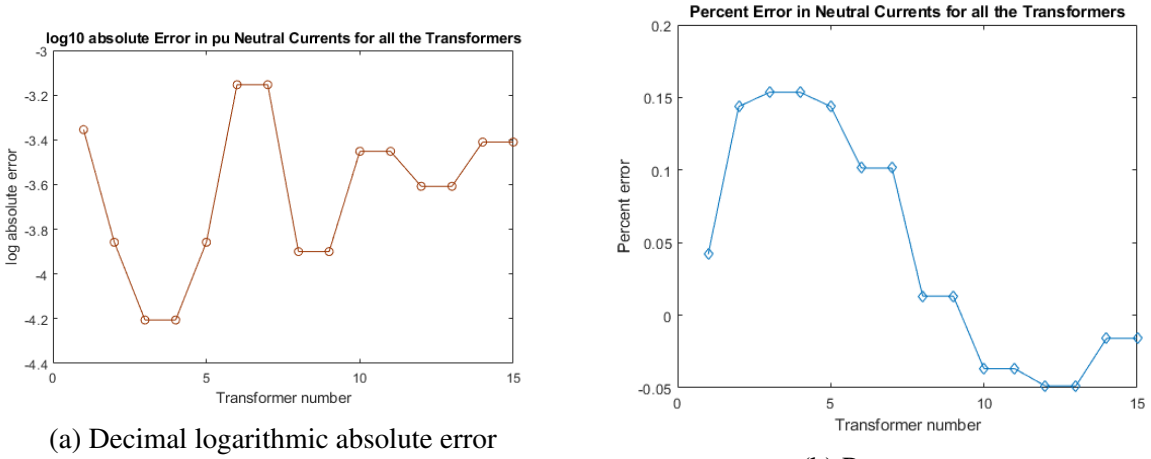

(a) Decimal logarithmic absolute error

(b) Percent error

Figure 4.4: Uniform electric field : 3V/km at 20°

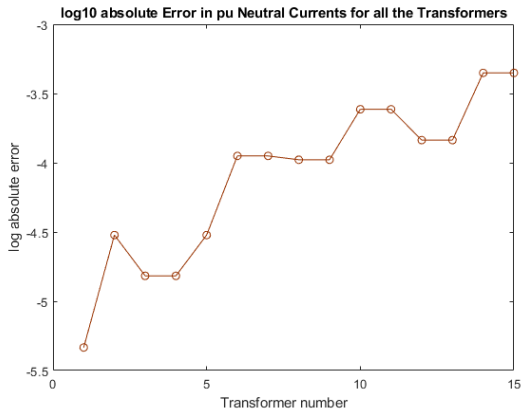

(a) Decimal logarithmic absolute error

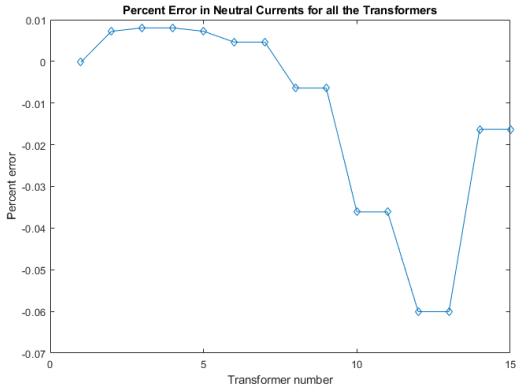

(b) Percent error

Figure 4.5: Uniform electric field : 4V/km at 220°

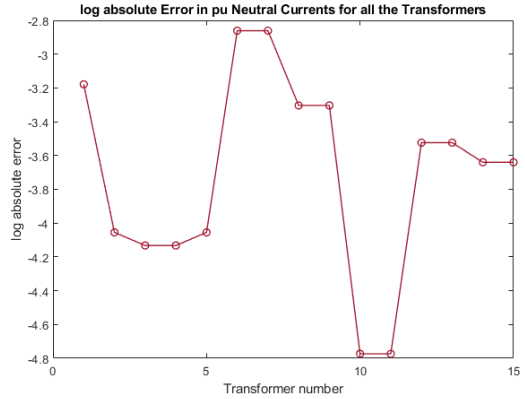

(a) Decimal logarithmic absolute error

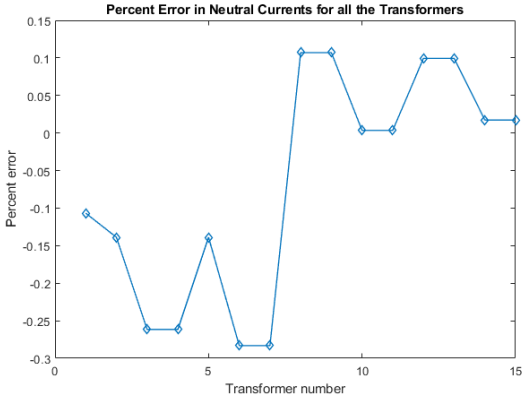

(b) Percent error

Figure 4.6: Non-uniform electric field for EPRI 20: Case 1

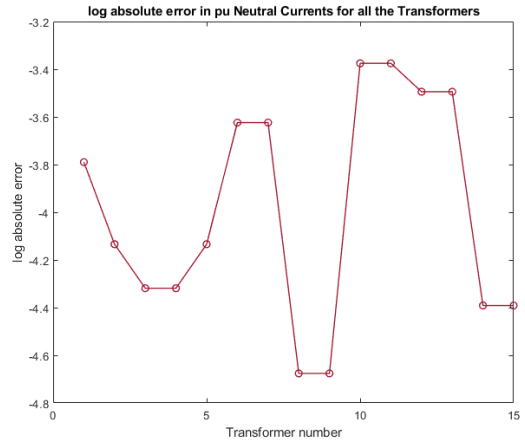

(a) Decimal logarithmic absolute error

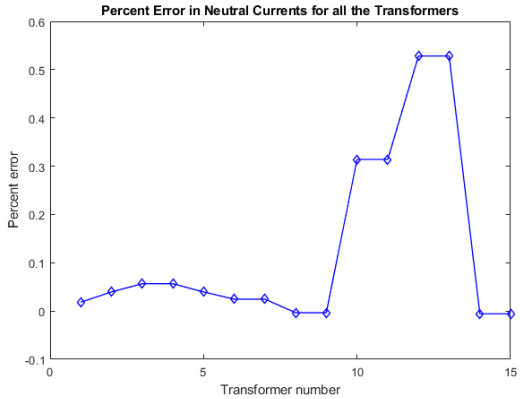

(b) Percent error

Figure 4.7: Non-uniform electric field for EPRI 20: Case 2

3.2 UIUC 150 bus

The tool is used on the 500/345 kV 150-bus system depicted in Fig. 3.2. Many electric field scenarios were applied out of which four have been depicted in the figures below. The scenarios were as follows:

1. Uniform electric field of magnitude 2.5 V/km at 0°.
2. Uniform electric field of magnitude 4 V/km at 20°.
3. Non uniform electric field - Case 1

Lat	Lon: -90.500	Lon: -90.000	Lon: -89.500	Lon: -89.000	Lon: -88.500	Lon: -88.000	Lon: -87.500	Lon: -87.000	Lon: -86.500	Lon: -86.000
36.500	0.850, 2.150	0.800, 2.150	0.750, 2.150	0.700, 2.150	0.650, 2.150	0.650, 2.150	0.600, 2.150	0.600, 2.150	0.550, 2.150	0.550, 2.150
36.000	0.850, 2.050	0.800, 2.050	0.750, 2.050	0.700, 2.050	0.650, 2.050	0.650, 2.050	0.600, 2.050	0.600, 2.050	0.550, 2.050	0.550, 2.050
35.500	0.850, 1.950	0.800, 1.950	0.750, 1.950	0.700, 1.950	0.650, 1.950	0.650, 1.950	0.600, 1.950	0.600, 1.950	0.550, 1.950	0.550, 1.950
35.000	0.850, 1.850	0.800, 1.850	0.750, 1.850	0.700, 1.850	0.650, 1.850	0.650, 1.850	0.600, 1.850	0.600, 1.850	0.550, 1.850	0.550, 1.850

Lon: -85.500	Lon: -85.000	Lon: -84.500	Lon: -84.000	Lon: -83.500	Lon: -83.000	Lon: -82.500	Lon: -82.000	Lon: -81.500
0.500, 2.150	0.500, 2.150	0.450, 2.150	0.450, 2.150	0.400, 2.150	0.400, 2.150	0.350, 2.150	0.350, 2.150	0.300, 2.150
0.500, 2.050	0.500, 2.050	0.450, 2.050	0.450, 2.050	0.400, 2.050	0.400, 2.050	0.350, 2.050	0.350, 2.050	0.300, 2.050
0.500, 1.950	0.500, 1.950	0.450, 1.950	0.450, 1.950	0.400, 1.950	0.400, 1.950	0.350, 1.950	0.350, 1.950	0.300, 1.950
0.500, 1.850	0.500, 1.850	0.450, 1.850	0.450, 1.850	0.400, 1.850	0.400, 1.850	0.350, 1.850	0.350, 1.850	0.300, 1.850

Figure 4.8: UIUC 150 - Case 1

4. Non uniform electric field - Case 2

Lat	Lon: -90.500	Lon: -90.000	Lon: -89.500	Lon: -89.000	Lon: -88.500	Lon: -88.000	Lon: -87.500	Lon: -87.000	Lon: -86.500	Lon: -86.000
36.500	1.500, 0.750	1.450, 0.750	1.400, 0.750	0.000, 0.750	1.300, 0.750	1.250, 0.750	1.200, 0.750	1.150, 0.750	1.100, 0.750	1.050, 0.750
36.000	1.500, 0.800	1.450, 0.800	1.400, 0.800	0.000, 0.800	1.300, 0.800	1.250, 0.800	1.200, 0.800	1.150, 0.800	1.100, 0.800	1.050, 0.800
35.500	1.500, 0.850	1.450, 0.850	1.400, 0.850	0.000, 0.850	1.300, 0.850	1.250, 0.850	1.200, 0.850	1.150, 0.850	1.100, 0.850	1.050, 0.850
35.000	1.500, 0.900	1.450, 0.900	1.400, 0.900	1.350, 0.900	1.300, 0.900	1.250, 0.900	1.200, 0.900	1.150, 0.900	1.100, 0.900	1.050, 0.900

Lon: -85.500	Lon: -85.000	Lon: -84.500	Lon: -84.000	Lon: -83.500	Lon: -83.000	Lon: -82.500	Lon: -82.000	Lon: -81.500
1.000, 0.750	0.950, 0.750	0.900, 0.750	0.850, 0.750	0.800, 0.750	0.750, 0.750	0.700, 0.750	0.650, 0.750	0.600, 0.750
1.000, 0.800	0.950, 0.800	0.900, 0.800	0.850, 0.800	0.800, 0.800	0.750, 0.800	0.700, 0.800	0.650, 0.800	0.600, 0.800
1.000, 0.850	0.950, 0.850	0.900, 0.850	0.850, 0.850	0.800, 0.850	0.750, 0.850	0.700, 0.850	0.650, 0.850	0.600, 0.850
1.000, 0.900	0.950, 0.900	0.900, 0.900	0.850, 0.900	0.800, 0.900	0.750, 0.900	0.700, 0.900	0.650, 0.900	0.600, 0.900

Figure 4.9: UIUC 150 - Case 2

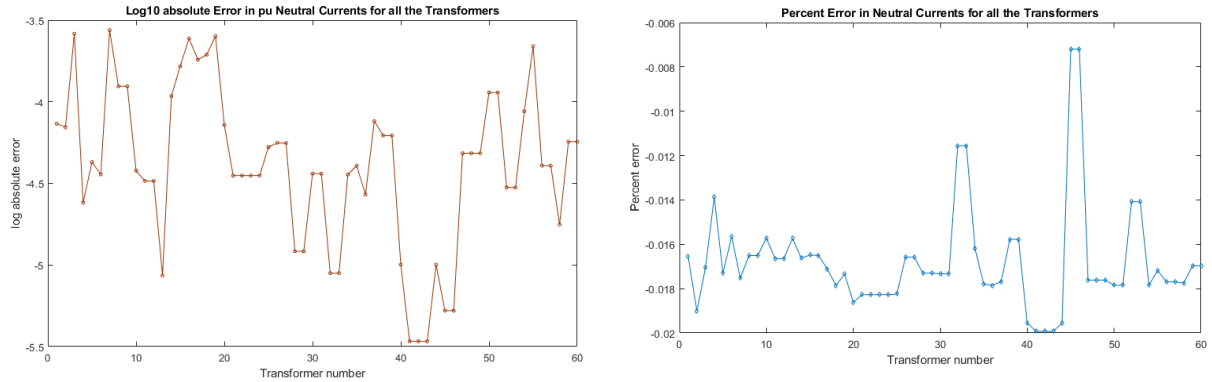

(a) Decimal logarithmic absolute error

(b) Percent error

Figure 4.10: Uniform electric field : 2.5V/km at 0°

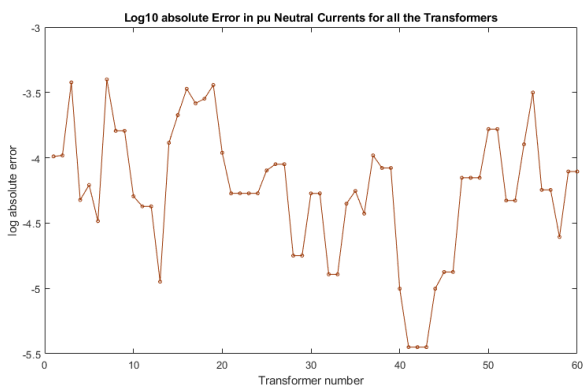

(a) Decimal logarithmic absolute error

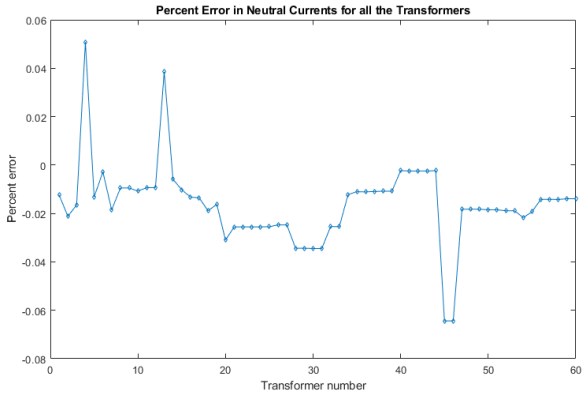

(b) Percent error

Figure 4.11: Uniform electric field : 4V/km at 20°

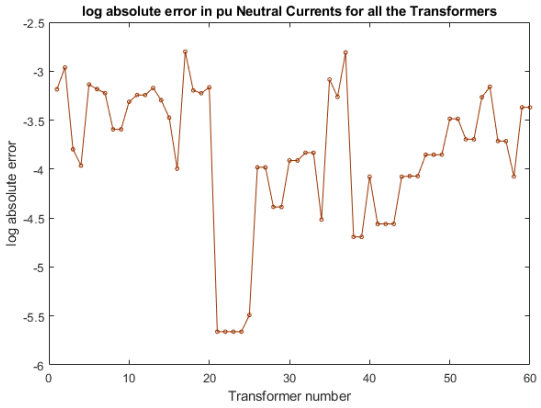

(a) Decimal logarithmic absolute error

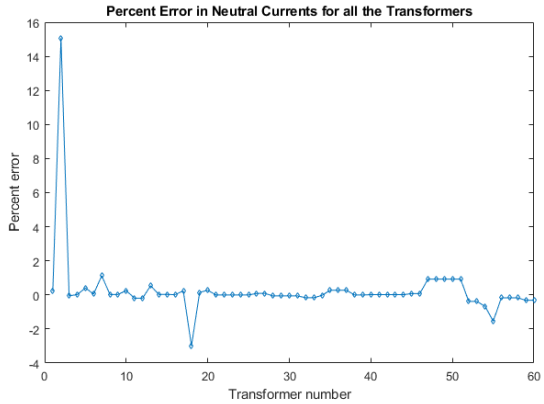

(b) Percent error

Figure 4.12: Non-uniform electric field for UIUC 150: Case 1

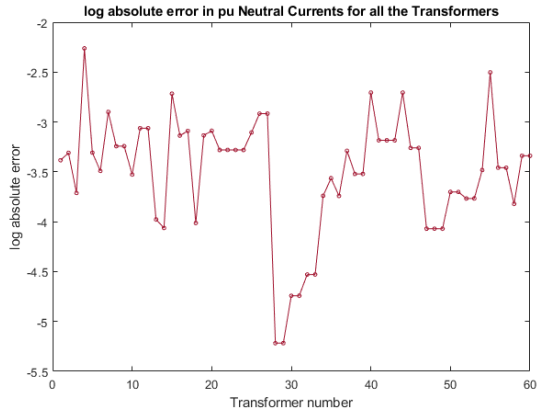

(a) Decimal logarithmic absolute error

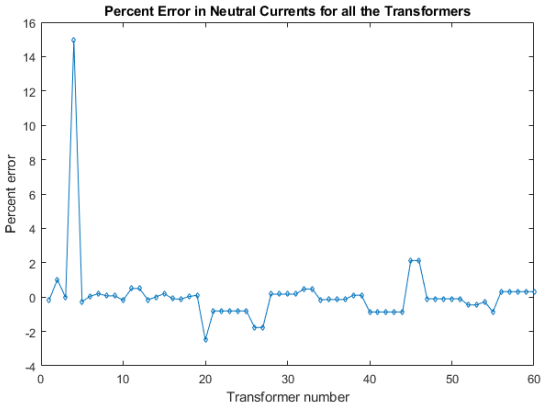

(b) Percent error

Figure 4.13: Non-uniform electric field for UIUC 150: Case 2

4 Interpretation

From the results of the above GMD scenarios, it can be inferred that the overall error in the computation of pu neutral GICs is small. For all the cases depicted in the last section, the decimal logarithmic error is in the range of -5.5 to - 2.5 which implies that the magnitude of error is around or less than 10^{-3}. The percent error is also less that 5%, with the maximum observed around 2% except for two isolated cases where the percent error is around 16%. For these two cases, after a close study, it has been observed that neutral GIC values were small (around 2 Amps) and even a slight error resulted in a percent error of greater magnitude.

Overall, MATGMD computes the neutral GICs with convincing accuracy for several GMD events. By interpolating this accuracy to other system parameters like the dc G matrix, injection currents, dc node voltages, transformer neutral currents, and effective GICs, we can say that these values can also be extracted with minimal error for various GMD studies pertaining to reliability, mitigation and estimation. For example, the GIC-inclusive state estimator will be heavily benefited from MATGMD and the availability of dc node voltages along with GIC values can aid the development of mitigation techniques. Additionally, the tool is equipped with the functionalities for calculating various parameters for both uniform as well as non-uniform electric field. Most GMD events result in non-uniform electric field and the ability of the tool to analyze the system for non-uniform electric field scenarios is a valuable addition. This capability has increased the applicability of MATGMD by many-folds for various, detailed GMD studies.

The MATGMD package can be found at https://github.com/gandhalijuvekar/MATGMD.

5. GIC-INCLUSIVE POWER SYSTEM STATE ESTIMATOR FOR GMD EVENTS

1 Introduction

Visibility of the system is an important facet for deciding the operator actions. This 'visibility' can be provided through system states that further help compute all the system values like flows and injections. As concluded in Chapter 3, a GIC inclusive state estimator is a potential solution to the power system state estimation problem encountered during the GMD events.

With the development of MATGMD, the computation of the additional reactive power losses using the effective GICs in the transformer during a GMD event is now possible. Additionally, good initial or starting values can also be calculated for the transformer neutral GICs states using this tool. This chapter details the development of the GIC-inclusive or modified state estimator along with the integration of the tool, MATGMD. The idea for the formulation is explained, the algorithm is described and the results showing verification using PowerWorld simulator for a few cases are depicted. The shortcomings in the formulation and application of the new estimator are mentioned and elucidated.

2 Modelling Scheme

From Chapter 2, we know that the GICs flowing in the system have the ability to cause half cycle saturation in the transformers present in the system. This half cycle saturation results in additional reactive power losses in these transformers which can be expressed using eq. 2.7. It is important to note that the equation shows the linear dependency of the reactive power loss on the effective GIC for the corresponding transformer. This reactive power additionally absorbed is not accounted for in the system model in eq. 2.8 for the state estimator. That is, the flows, injections, line losses, generator outputs, etc., are not updated. Hence, the system model needs to account for these changes. The algorithm has been developed using MATPOWER state estimation package [51] as its base code with modifications to accommodate the changes that are entailed for the GIC-inclusive state estimator.

2.1 Shortcomings of Plan I

Accounting these losses would require their calculation being enabled in the state estimation system model. An obvious first choice for facilitating this would be to append the effective GICs to the system state vector along with voltage angle and magnitude. Along with the changes in the state vector, the measurement vector also needed to be changed for the sake of accuracy and observability. Hence, it was changed by the addition of effective GICs as measurements. The measurement values were obtained from PowerWorld Simulator and Gaussian noise was added. The model was changed to account for the reactive power losses and tested. The output was as expected, the error in the voltage angle and magnitude states reduced drastically validating the changed model. But there was an issue! - The GIC measurements obtained in the physical world through GIC monitoring devices placed at the substations are that of the transformer neutral GICs. The effective GIC is not an actual, measured value but is a calculated value according to eq. 2.6 for computation of the additional reactive power losses in the transformers. Since, measurements cannot be directly obtained for the effective GICs, it is not ideal to have the measurement vector comprise of effective GICs. At the same time, for a given electric field or its estimate, the transformer neutral GICs are computed before the computation of GICs. Also, neutral GICs can be used to calculate the values of effective GICs but not vice-versa. Hence, making transformer neutral GICs states for the estimator is a better choice than the effective GICs.

2.2 Shortcomings of Plan II

Next, transformer neutral GICs were appended to the traditional states for the GIC-inclusive state estimator. At the same time, the neutral GICs were also included in the measurement vector making sure that the observability criteria is met. The new system model was developed and implemented in the state estimator code. Tests for various electric field scenarios were carried out and the output was verified with PowerWorld Simulator output. The error was similar to that of the previous case - small. Hence, this model was validated, too. But again, there was another issue observed - the conditioning number of the Jacobian matrix, $\mathbf{H}$ was in the order of 10^{13} indicating

ill-conditioning. This can cause potential convergence issues in bigger cases or might need higher number of iterations to converge to a solution. A solution that could alleviate this issue would be the use of pu transformer neutral GICs as the states instead of transformer neutral GICs as well as the inclusion of pu transformer neutral GICs as measurements.

2.3 Plan III

Finally, the pu transformer neutral GICs were appended as states to the traditional states for the modified state estimator. The measurement vector also included the pu neutral GICs values as available measurements for observability and accuracy in the estimation. The states can be visualised as $\mathbf{x} = [\theta, \mathbf{V_m}, \mathbf{I_{n,pu}}]^T$ where, θ is the set of all bus angles, $\mathbf{V_m}$ is the set of all bus voltage magnitudes in pu and $\mathbf{I_{n,pu}}$ is the set of all pu transformer neutral GICs. The measurements can be visualised as, $\mathbf{z_i} = [\mathbf{P_{flows}}, \mathbf{P_{inj}}, \theta_{\mathbf{meas}}, \mathbf{Q_{flows}}, \mathbf{Q_{inj}}, \mathbf{V_{meas}}, \mathbf{I_{meas}}]^T$ where, $\mathbf{P_{flows}}$ and $\mathbf{Q_{flows}}$ is the set of real and reactive power flows measured, respectively, $\mathbf{P_{inj}}$ and $\mathbf{Q_{inj}}$ is the set of real and reactive power injections measured, respectively, $\theta_{\mathbf{meas}}$ is the set of voltage angles measured, $\mathbf{V_{meas}}$ is the set of voltage magnitudes measured and $\mathbf{I_{meas}}$ is the set of pu transformer neutral GICs measured.

The changes in the model for the estimator can be explained as follows:

1. Changes in the estimates of the reactive power flows from the high (from) voltage side to the low (to) voltage side for transformer branches and injections at the high side transformer bus (for the estimator I developed, high side bus refers to from side transformer bus because PowerWorld models these additional losses on the from side bus instead of the high side. And as mentioned before, the verification of the accuracy is done using PowerWorld).

   - After accounting of the reactive power losses in the transformers, the estimates can be expressed as follows:

$$Q_{inj,i,new} = Q_{inj,i,initial} + Q_{loss,i} \tag{2.1}$$

$$Q_{flow,ij,new} = Q_{flow,ij,initial} + Q_{loss,ij} \tag{2.2}$$

   where, $Q_{inj,i,new}$ is the new reactive power loss injection estimate at the from side bus i,

$Q_{inj,i,initial}$ is the traditional (from the power flow equations) reactive power loss injection estimate at the from side bus i, $Q_{loss,i}$ is the additional reactive power loss in the transformer from eq. 2.7 modeled at the from side bus i, $Q_{flow,ij,new}$ is the new reactive power loss flow estimate for branch from bus i to bus j, $Q_{flow,ij,initial}$ is the traditional (from the power flow equations) reactive power loss flow estimate for branch from bus i to bus j,and $Q_{loss,ij}$ is the additional reactive power loss in the transformer branch from bus i to bus j.

2. Changes in the terms of the Jacobian matrix, **H** because of the eq. 2.7 relationship belong to two categories. One, the new partial differentiation terms that define the relationship between the reactive power flows and injections to the pu transformer neutral GICs system states. Two, the additional partial differentiation terms that get added to the original terms that relate reactive power flows and injection to the pu voltage magnitude state. These two changes occur because the additional reactive power loss is linearly dependent on the pu voltage magnitude at the high (from) side transformer bus and the pu transformer neutral GIC. Before divulging into the details of these terms, it is important to derive one more expression - that of the partial differentiation of the pu effective GIC to the pu neutral GIC for a given transformer. It can be derived as follows:

$$I_{eff,tr_k} = \mid I_{h,tr_k} + I_{l,tr_k}/a_{tr_k} \mid \tag{2.3}$$

$$I_{eff,pu,tr_k} = \mid I_{n,pu,tr_k} \times (r_{h,tr_k} + r_{l,tr_k}/a_{tr_k}) \mid \tag{2.4}$$

$$\partial I_{eff,pu,tr_k}/\partial I_{n,pu,tr_k} = \pm(r_{h,tr_k} + r_{l,tr_k}/a_{tr_k}) \tag{2.5}$$

where, I_{eff,tr_k} is the effective GIC, I_{h,tr_k} is the high side GIC, I_{l,tr_k} is the low side GIC, I_{n,tr_k} is the neutral GIC, r_{h,tr_k} and r_{l,tr_k} are the ratios of high side and low side GICs respectively to the neutral GIC, and a_{tr_k} is the transformer turns ratio for transformer k.

The new and additional terms can be expressed as:

(a) New partial differentiation terms in the Jacobian matrix, **H**:

$$\partial Q_{inj,i}/\partial I_{n,pu,tr_k} = V_{pu,i} \times k_{pu,tr_k} \times (\partial I_{eff,pu,tr_k}/\partial I_{n,pu,tr_k}) \tag{2.6}$$

$$\partial Q_{flow,ij}/\partial I_{n,pu,tr_k} = V_{pu,i} \times k_{pu,tr_k} \times (\partial I_{eff,pu,tr_k}/\partial I_{n,pu,tr_k}) \tag{2.7}$$

where, $\partial Q_{inj,i}/\partial I_{n,pu,tr_k}$ and $\partial Q_{flow,ij}/\partial I_{n,pu,tr_k}$ are the partial differentiation terms relating the injections and flows respectively to the pu neutral GIC of a transformer k, $V_{pu,i}$ is the pu voltage magnitude at the high (from) side transformer bus, k_{pu,tr_k} is the scalar transformer parameter for transformer k, n_x is the number of transformers in the system and $\partial I_{eff,pu,tr_k}/\partial I_{n,pu,tr_k}$ is the partial differentiation term that can be substituted from eq. 2.5.

(b) Additional partial differentiation terms in the Jacobian matrix, **H**:

$$\partial Q_{inj,i}/\partial V_{pu,i} = \sum_{k=1}^{n_x} k_{pu,tr_k} \times I_{eff,pu,tr_k} \tag{2.8}$$

$$\partial Q_{flow,ij}/\partial V_{pu,i} = k_{pu,tr_k} \times I_{eff,pu,tr_k} \tag{2.9}$$

where, $\partial Q_{inj,i}/\partial V_{pu,i}$ and $\partial Q_{flow,ij}/\partial V_{pu,i}$ are the partial differentiation terms relating the injections and flows respectively to the pu voltage magnitude of the high (from) side bus of a transformer k and I_{eff,pu,tr_k} is the pu effective GIC that can be substituted from eq. 2.4.

It is important to note that the values of I_{eff,pu,tr_k}, r_{h,tr_k} and r_{l,tr_k} are obtained from the tool, MATGMD which is integrated in the state estimator code at various locations and runs for every iteration. Aside from these values, the tool is also used to compute the initial/starting values of the pu neutral GICs and hence, placed in the code to execute this job. Here, the assumption is that the electric field information or estimate is fairly accurate and the ac GIC-inclusive state estimator does not dwell in the area of electric field estimation.

2.4 Flowchart for Formulation

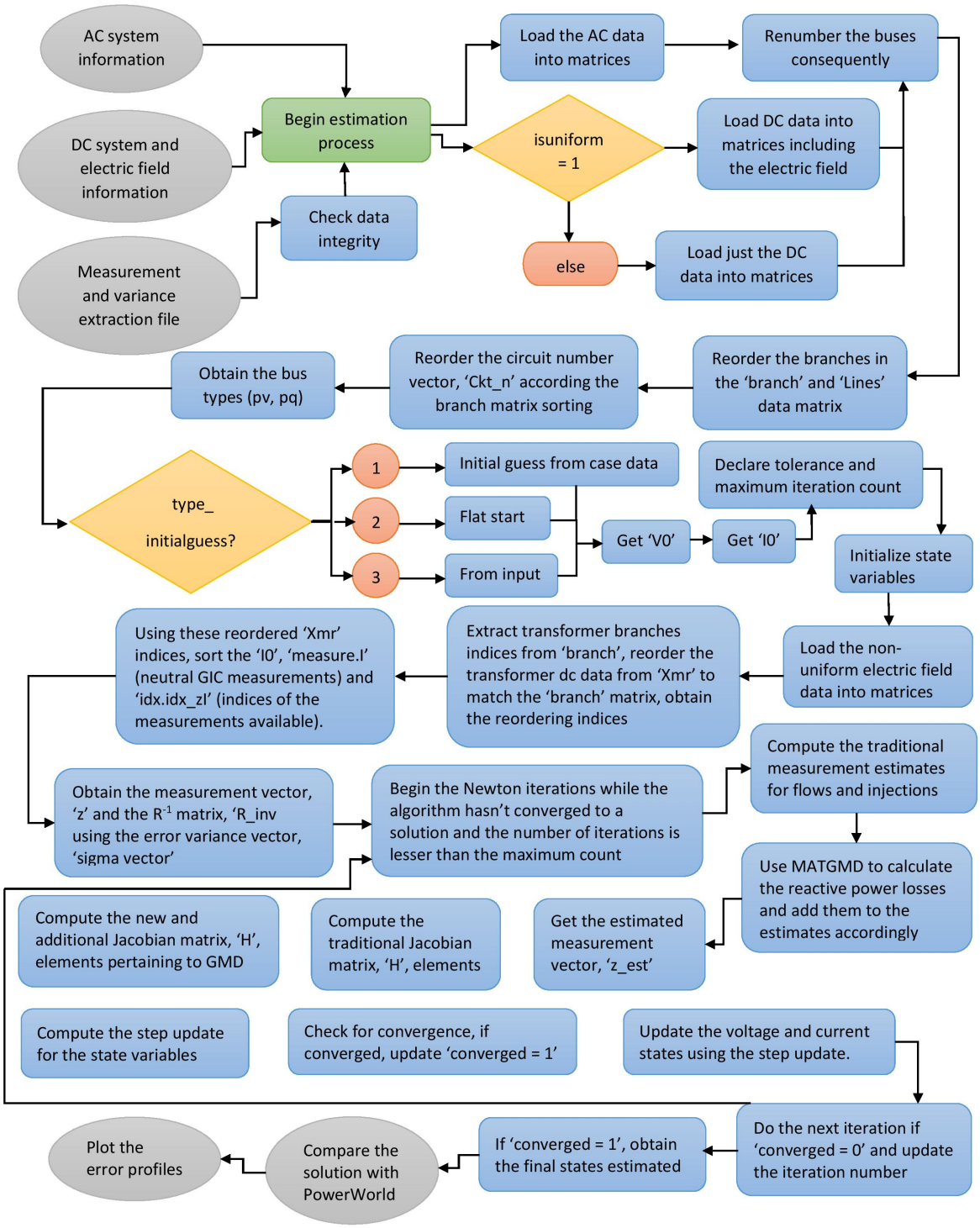

Figure 5.1: Formulation algorithm flowchart

2.5 Function Files Involved and their Application

The flowchart on the last page explains the formulation procedure of the ac GIC-inclusive state estimator along with the procedure to verify its accuracy using the PowerWorld Simulator. The implementation of this procedure involves execution of various function files in order. The files modified from MATPOWER and additional files developed are detailed as follows:

1. Test file: **testse_gic_XXXX.m**

   The 'XXXX' refers to the abbreviation of the case name. This file extracts the information from the measurement file, the system case input files pertaining to both ac (same as the input file used by MATPOWER) and dc (as detailed in the last chapter) system as well as the electric field. It checks the integrity of the measurement data obtained. It requires additional information about whether the electric field is uniform and the type of initial guess that would be used for states. It also includes the file that runs the state estimation. Once the outputs are obtained, the file plots the error profile. Verification of the state estimation output could be done in various ways and hence, it is customizable.

2. Measurement file: **measGen_XX.m**

   The 'XX' refers to the abbreviation or extension the user would like to give the measurement file for different system cases, the base of these files being the core file - measGen.m. The measurement file extracts actual system values from excel sheets using the file directory. An option to add noise based on the variance (ultimately linking to the weighting factors) and include voltage angle measurements is provided. The files are opened and the relevant values are extracted. The buses and branches as well as their corresponding data is sorted in order of the increasing bus numbers. If the option to add noise is enabled, Gaussian noise is added. Required fractions of each measurement type is declared and is used to randomly select the data.

3. Run state estimation file: **run_se_GICn.m**

   This file is built on the original MATPOWER run_se.m file. Apart from it's original func-

tionality, there are a few more tasks it performs to enable state estimation for GMD studies. It loads the dc system and electric field information if the field is uniform. All the extracted information is reordered according to bus numbers for both buses and branches. This information is passed through the function file that actually does (runs) the state estimations and outputs the result for the system states. These output states are then subtracted from the actual state values obtained from PowerWorld and the absolute of these values is given as one of the outputs of the run_se_GICn.m file for further computations and plotting in the test file.

4. Loading the dc system data for GMD: **loadGMD.m**

   This file loads the dc system information from the dc case file for the given system. It is based on the loadcase.m function file from MATPOWER that loads the ac system information from the ac case file for the given system. Inconsistencies in the case file can be recognized, too.

5. Renumbering buses: **ext2int_dc.m**

   This function file renumbers the buses from the dc system data consecutively if they aren't numbered in a consecutive fashion. It follows the function file ext2int.m that performs this functionality for the ac system data.

6. Doing state estimation: **doSE_GICn.m**

   This function actually performs the state estimation by taking in all the system information extracted using various function files in the run_se_GICn.m file as its input. It declares iteration parameters such as tolerance, maximum iterations and also decides on the initial or starting values for the estimation based on the user input. For a non uniform electric field, the data is extracted. The transformer branches are recognised from the set containing all the branches. The transformer dc information matrix is rearranged according to the index of the transformer branches in the ac system information and a vector with rearranged indices is obtained. This vector is then used to rearrange the initial or starting pu neutral current values and the measurement pu neutral current values, accordingly. The ratios of the high side cur-

rent and the low side current to the neutral current are obtained using the function files from the tool, MATGMD. Beginning with the starting pu neutral current values, the pu effective GICs are obtained from the ratios and from the updated pu neutral current at every iteration performed during the estimation. Using the pu effective GICs, the additional reactive power losses in the transformers are computed and the estimates of the measurements are obtained. Next, the new and additional terms that would occupy the Jacobian matrix, **H** are calculated according to eq. 2.6, 2.7, 2.8 and 2.9. The iteration is performed and the state vector gets updated.

7. Loading the electric field data for a non-uniform electric field: **loadEfield.m**

   If the is_uniform flag is down, the non-uniform electric field data is extracted using the loadEfield.m function file which works like loadcase.m and loadGMD.m but for loading the non-uniform electric field information.

8. Obtain transformer branches and the sorting order for rearranged dc transformer data matrix: **Xmr_branch.m**

   The indices of the transformer branches are obtained by first identifying the transmission lines using circuit numbers and are one of the outputs. Using these indices, the dc transformer data matrix is sorted (and sent as output, too) in the order that is present in the ac transformer branches and the order of this sorting is sent as an output to sort the pu neutral GICs and their measurements.

9. Computation of the estimates of the additional reactive power loss flows: **Qloss_br.m**

   The additional reactive power loss at every transformer branch is computed according to eq. 2.7 and is assigned to the from vector of the transformer branch additional reactive flow measurement estimates.

10. Computation of the estimates of the additional reactive power loss injections: **Qloss_bus.m**

    The additional reactive power loss modeled at every transformer high (from) side bus is computed which is the summation of all the additional losses at every transformer which

has this bus connected to its high (from) side and is assigned to the vector containing these additional loss injection estimates.

11. New partial differentiation terms for the relationship between flows and the neutral currents: **dQlossbr_dI.m**

    The partial differentiation term relating the transformer branch flows for both high (from) and low (to) bus to the transformer neutral GICs is computed according to eq. 2.7. Two matrices of dimensions 'number of branches $\times$ number of transformers' corresponding to the from flows and to flows are initialized to zero and every relation computed is assigned to the matrices accordingly. It is important to remember that these terms are the new terms that get appended to the traditional Jacobian matrix, **H**.

12. New partial differentiation terms for the relationship between injections and the neutral currents: **dQlossbus_dI.m**

    The partial differentiation term relating the high (from) side bus injections to the transformer neutral GICs is computed according to eq. 2.6. A matrix of dimensions 'number of buses $\times$ number of transformers' corresponding to the system buses is initialized to zero and every relation computed is assigned to the matrix accordingly. These terms are the new terms that get appended to the traditional Jacobian matrix, **H**.

13. Additional partial differentiation terms for the relationship between flows and the voltage magnitudes: **dQlossbr_dVm.m**

    The partial differentiation term relating the transformer branch flows for both high (from) and low (to) bus to the high (from) bus voltage magnitudes is computed according to eq. 2.9. Two matrices of dimensions 'number of branches $\times$ number of buses' corresponding to the from flows and to flows are initialized to zero and every relation computed is assigned to these matrices accordingly. It is important to remember that these terms get added to the traditional terms that relate flows to the voltage magnitudes.

14. Additional partial differentiation terms for the relationship between injections and the volt-

age magnitudes: **dQlossbus_dVm.m**

The partial differentiation term relating the high (from) side bus injections to the high (from) side bus voltage magnitudes is computed according to eq. 2.6. A matrix of dimensions 'number of buses $\times$ number of buses' corresponding to the system buses is initialized to zero and every relation computed is assigned to the matrix accordingly. These terms get added to the traditional terms that relate injections to the voltage magnitudes.

The above described files are either new files or files that have undergone change from the original MATPOWER files to accommodate the GMD state estimation functionality.

3 Test Case Description and Results

The analysis for the state estimation was carried out on the 500/345 kV EPRI 20-bus system depicted in Fig. 4.3. Currently, efforts are being taken to perform these analysis on the UIUC 150-bus system and eventually on the Texas 2000-bus system. Various types of GMD scenarios were simulated on PowerWorld but the results below depict only a few of the tested cases for inference purposes. The cases tested are the following ones:

1. One uniform electric field scenarios,
2. Two non-uniform electric field scenarios,
3. Uniform electric field of increasing magnitude (3V/km to 9V/km) at a fixed direction (0°),
4. Uniform electric field of fixed magnitude (3V/km) and varying direction from 0 - 360 degrees.

For scenarios of type (1) and (2), the decimal logarithm of the average absolute error is plotted for two state (Voltage magnitude and transformer neutral GICs) individually over a 100 Monte-Carlo simulations. For scenarios of type (3) and (4), the decimal logarithm of the total average absolute error, comprising of the errors for all the states, is plotted for every scenario (changing magnitudes with fixed direction and changing directions with fixed magnitude) individually over a 100 Monte-Carlo simulations.

3.1 Uniform electric field with magnitude 7 V/km and direction 0 degrees

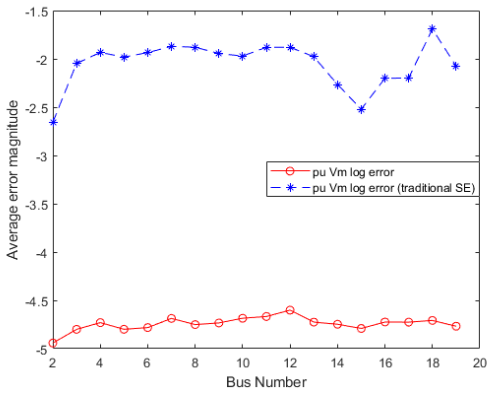

(a) Decimal logarithmic absolute error comparison for the voltage magnitude state

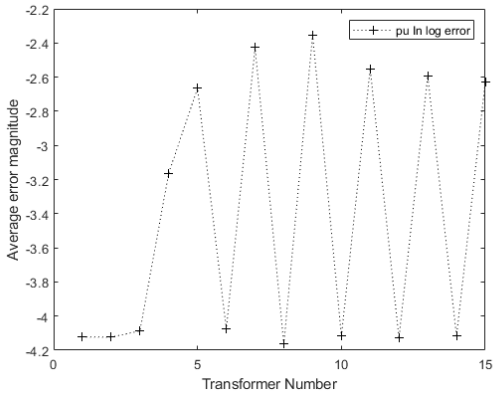

(b) Decimal logarithmic absolute error for the neutral GIC state

Figure 5.2: Neutral GIC measurements taken only at one transformer if many transformers with the same parameters are in parallel

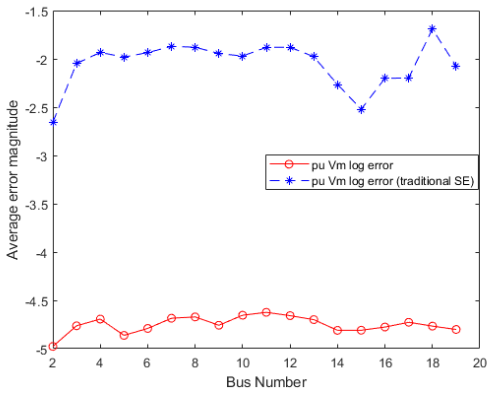

(a) Decimal logarithmic absolute error comparison for the voltage magnitude state

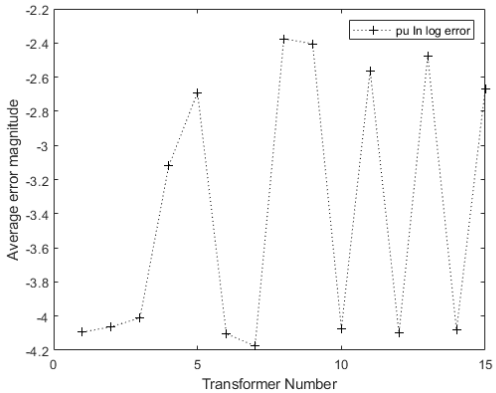

(b) Decimal logarithmic absolute error for the neutral GIC state

Figure 5.3: Neutral GIC measurements taken taken at random with the percentage of measurements kept at 50% of the total

The figs. 5.2 and 5.3 represent the error in the voltage magnitude and the neutral current state (in pu) for two different cases as detailed above. For both cases, the voltage magnitude state error at every bus is below $10^{-4.5}$. For the neutral current state estimates, the error is below $10^{-2.2}$ for both cases and the error in the estimation of currents at the 8^{th} and 9^{th} transformers is higher (as expected) because of the absence of measurements at both the transformers.

3.2 Non-uniform electric field: Case 1

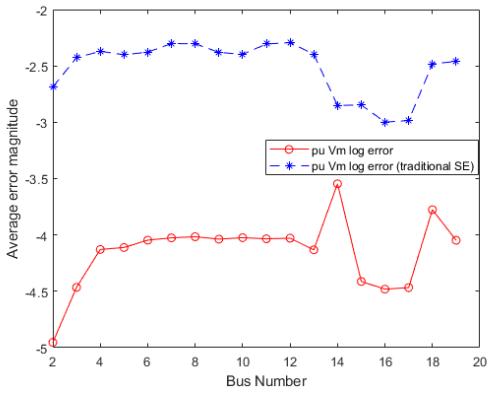

(a) Decimal logarithmic absolute error comparison for the voltage magnitude state

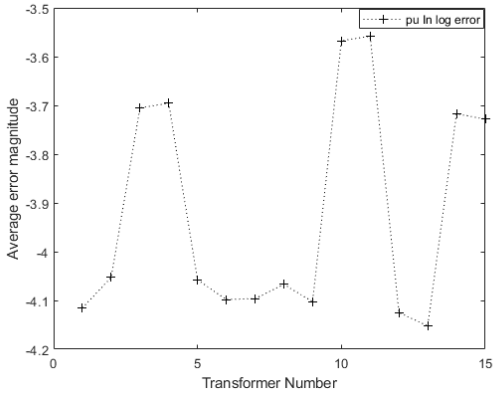

(b) Decimal logarithmic absolute error for the neutral GIC state

Figure 5.4: Non-uniform electric field : Case 1 - Neutral GIC measurements at three sets of parallel transformers are not given as measurement inputs

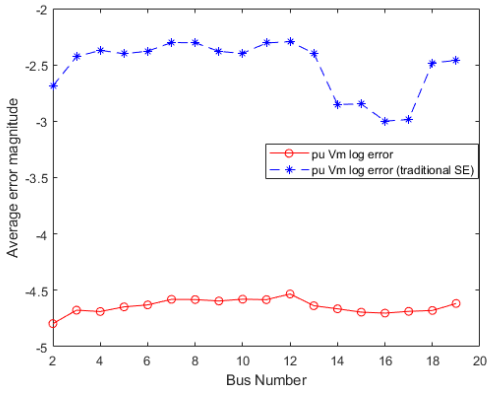

(a) Decimal logarithmic absolute error comparison for the voltage magnitude state

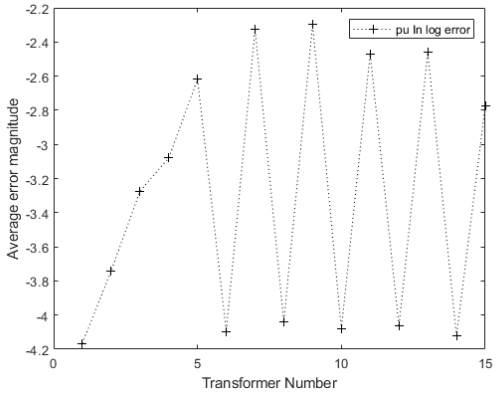

(b) Decimal logarithmic absolute error for the neutral GIC state

Figure 5.5: Non-uniform electric field : Case 1 - Neutral GIC measurements taken only at one transformer if many transformers with the same parameters are in parallel

The figs. 5.4 and 5.5 represent the error in the voltage magnitude and the neutral current state (in pu) for two different scenarios as detailed above. For both cases, the voltage magnitude state error is low: below $10^{3.5}$ for the first scenario and $10^{-4.5}$ for the second. For the neutral current state estimates, the error is below $10^{-2.2}$ for both cases. The error in the neutral current estimates at the 3 sets of parallel transformers devoid of measurements is higher (as expected). This even increases the error in the voltage magnitude estimates as seen in fig. 5.4a when compared to the error for fig. 5.5a which is the scenario with at least one measurement for a set of parallel transformers.

3.3 Non-uniform electric field: Case 2

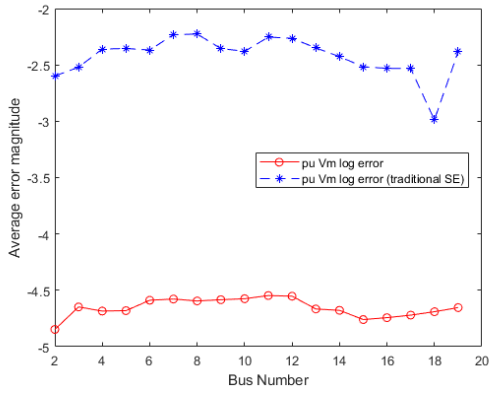

(a) Decimal logarithmic absolute error comparison for the voltage magnitude state

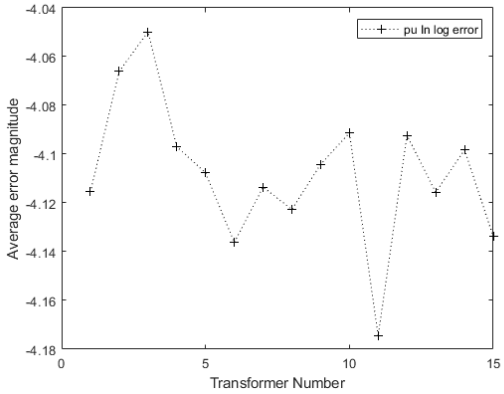

(b) Decimal logarithmic absolute error for the neutral GIC state

Figure 5.6: Non-uniform electric field : Case 2 - All neural GIC measurements

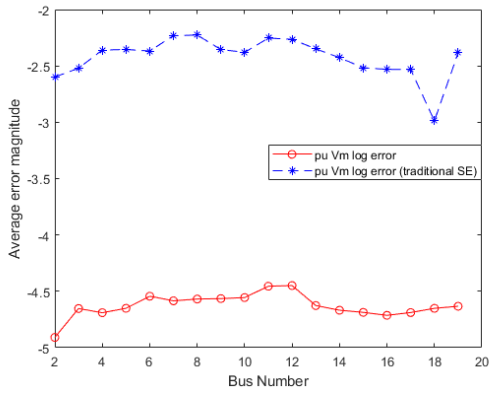

(a) Decimal logarithmic absolute error comparison for the voltage magnitude state

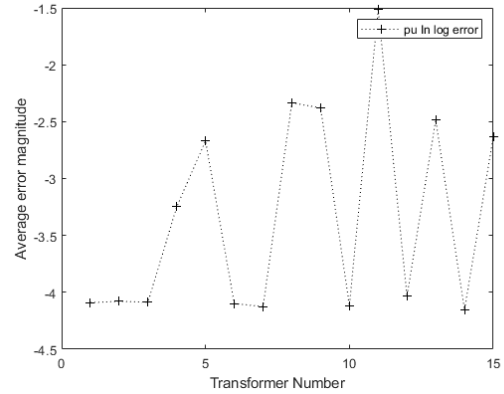

(b) Decimal logarithmic absolute error for the neutral GIC state

Figure 5.7: Non-uniform electric field : Case 2 - Neutral GIC measurements taken taken at random with the percentage of measurements kept at 50% of the total

The figs. 5.6 and 5.7 represent the error in the voltage magnitude and the neutral current state (in pu) for two different scenarios detailed above. For both cases, the voltage magnitude state error is below 10^{-4} but slightly higher for the second scenario. For the neutral current state estimates, the error is below 10^{-4} for the first scenario and below $10^{-1.5}$ for the second. These differences in the errors of the two states can be attributed to the availability of lesser neutral current measurements in the second scenario along with the fact that one set of parallel transformers (8^{th} and 9^{th}) do not have neutral current measurements available.

3.4 Uniform electric field of increasing magnitude (3V/km to 9V/km) at a fixed direction (0 degrees)

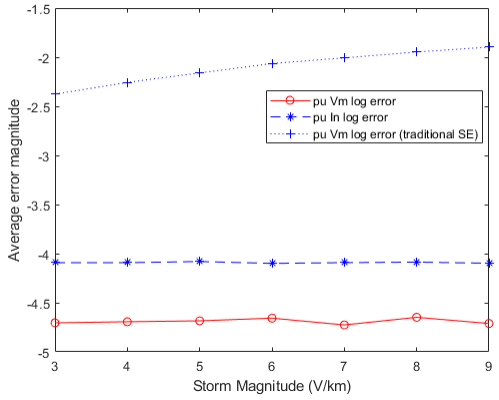

Figure 5.8: Decimal logarithmic absolute error for the voltage magnitude and neutral GIC states along with the voltage magnitude state error from the traditional state estimator

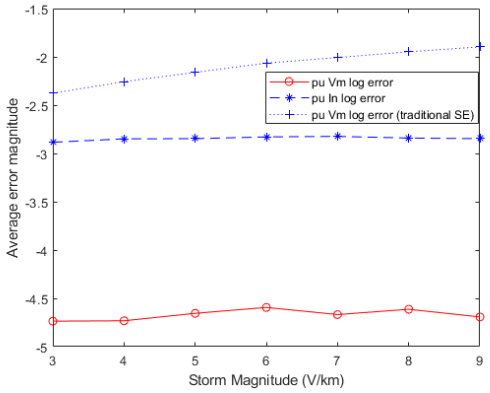

(a) Neutral GIC measurements taken only at one transformer if many transformers with the same parameters are in parallel

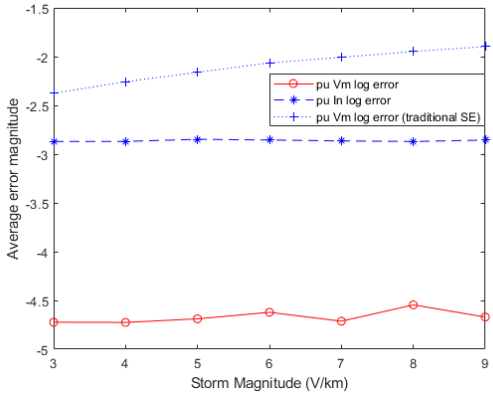

(b) Neutral GIC measurements taken taken at random with the percentage of measurements kept at 50% of the total

Figure 5.9: Decimal logarithmic absolute error for the voltage magnitude and neutral GIC states with lesser neutral GIC measurements along with the voltage magnitude state error from the traditional state estimator

The figs. 5.8, 5.9a and 5.9b depict the error profiles for the estimation of the voltage magnitude and neutral current states at different uniform electric field magnitudes ranging from 3 - 9V/km at a fixed direction. The error profile for the voltage magnitude state using a traditional power system estimator is also depicted for comparison. It can be observed that the error decreases significantly for all the three scenarios detailed above - it is consistently below $10^{-4.5}$. The neutral

current estimation error is much lower when all the measurements are available for estimation as compared to when only about 50% are available. A peculiar occurrence to note here is that despite the fact that measurements at a set of parallel transformers is not available for scenario in fig. 5.9b, the error profile is almost similar to that in scenario in fig. 5.9a where at least one measurement at a set of parallel transformers is available.

3.5 Uniform electric field of fixed magnitude (3V/km) and varying direction from 0 - 360 degrees

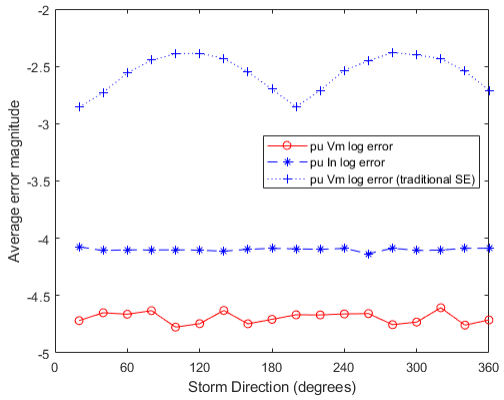

Figure 5.10: Decimal logarithmic absolute error for the voltage magnitude and neutral GIC states along with the voltage magnitude state error from the traditional state estimator

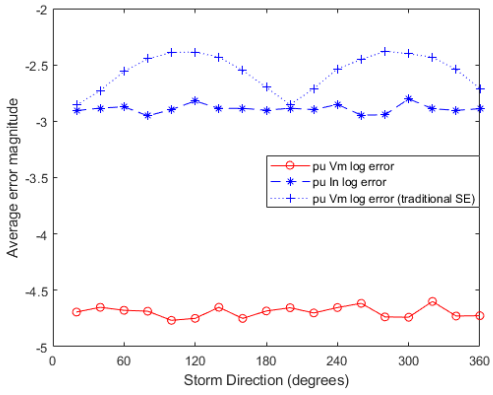

(a) Neutral GIC measurements taken only at one transformer if many transformers with the same parameters are in parallel

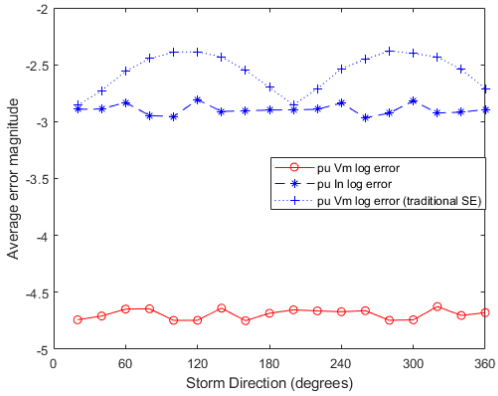

(b) Neutral GIC measurements taken taken at random with the percentage of measurements kept at 50% of the total

Figure 5.11: Decimal logarithmic absolute error for the voltage magnitude and neutral GIC states with lesser neutral GIC measurements along with the voltage magnitude state error from the traditional state estimator

The figs. 5.10, 5.11a and 5.11b depict the error profiles for the voltage magnitude and neutral current states at different uniform electric field directions ranging from 0 - 360° for a fixed magnitude. Similar to the varying magnitude case, it is observed that the voltage magnitude state error is consistently below $10^{-4.5}$ and the neutral current estimation error is much lower when all the measurements are available for estimation as compared to when only about 50% are available.

4 Conclusion

The various approaches taken towards handling the power system state estimation problem have been detailed in this chapter and their shortcomings have been explained. The modeling scheme has been explained describing the changes in various traditional model parameters along with the equations that are vital to the changed system model. The algorithm developed for the GIC-inclusive ac state estimator is illustrated using a flowchart to give a holistic understanding about the changed state estimator and parameters used to verify its relevance and accuracy. The functionalities of the modified and newly constructed function files have been elaborated. Efforts were taken to construct these function files so that the computation time was low and the computation accuracy was retained. The results indicate that the modified or GIC-inclusive state estimator does a great job with estimating the traditional as well as the new system states. It also solves the convergence problem that the traditional state estimation was marred with. That being said, there are still a few issues that need attention. One of them is the decision on the weighting factors to be utilized. Weighting factors pertaining to the traditional measurements can be obtained from the literature but for the newer neutral GIC measurements, obtaining these factors can get complicated requiring extensive studying of these measurements in the physical world. Another issue is parameter errors which also requires analysis in the physical world as mentioned in section 3.1. This would require a constantly updated dc system information file to be passed through the modified state estimation framework which can be done easily with slight revisions in the code. Lastly, the issue of observability is a complex one that would involve extracting information about certain hidden system relationships that could shed light on the dependencies of the states on the measurements for GMD scenarios.

6. CONCLUSIONS AND PROPOSED FUTURE WORK

1 MATGMD

As seen from chapter 4, the MATGMD package is an efficient tool that computes the GMD related system parameters with a good level of accuracy. Hence, it can find its use in various studies involving development of mitigation techniques, transient stability analysis, etc. A tool available at your disposal on MATLAB can save users the need to spend time on coding for these system values as MATGMD is easy to use and can adapt to any system case requirements. The speed of the computation is decent but could be improved by applying sparse matrix techniques. If need be, the tool can be exported, with some effort, to any other client enabling extensive application. The ability of the tool to perform analysis on both uniform and non-uniform electric field scenarios has widened its scope of utilization.

2 GIC-Inclusive AC State Estimator

As seen from chapter 5, the GIC-inclusive ac state estimator helps estimate the system states within working accuracy. This validates its modeling and implies that it could be used for state estimation applications for GMD scenarios over the traditional state estimator. The utilities and system operators can heavily benefit from using this estimator framework in their systems. Operator actions during events depend on the state estimation results and this visibility of the system during a potential large-scale GMD event could save the system from a collapse. Mitigation techniques may involve line switching, increasing the reactive power support, generator re-dispatch, etc and they require information about the 'situation' the system is in. During GMD events, this information can be obtained using the modified state estimator which outputs the system states that can ultimately help compute the information for the entire system. Hence, timely measures can be taken to curb the disastrous effects of GICs circulating during a GMD.

These advantages exist but they are accompanied by certain issues mentioned in section 4. Observability is crucial during the estimation process. The additional neutral current states aggravate

the situation. The rules that applied to the traditional state estimator do not apply to the modified ones as newer relationships govern observability. These relationships may ultimately help obtain the conditions for critical measurements.

Another area with the potential to boost the relevance and accuracy of the GIC-inclusive state estimator is usage of reliable electric field estimates for the given GMD scenario as a precursor to the GIC-inclusive ac state estimator. There is currently work being done at Texas A&M on such a dc GIC estimator that is aiming to get accurate electric field estimates from the magnetic field and earth data. A combination of both these estimators could give the system states as output using the magnetic field data. This would help us create a model that helps evaluate the real world models directly.

Another study that could help make decisions during GMD events is the accuracy of the neutral GIC measurements. As GIC monitors may not be installed at all the locations desired, pseudo-measurements with higher variance could be fed as measurements for retaining observability. It may be interesting to analyze what error variance of those measurements could give us acceptable results? To what extent does the accuracy depend on this variance? This could help direct the research for analysis of measurements required for the GIC-inclusive state estimator.

Overall, the GIC-inclusive state estimator would need multiple revisions and upgradations to accommodate various considerations and issues. But the primary model has shown the potential to solve the state estimation problem and hence, its application in the real world is imperative.

REFERENCES

[1] "Effects of Geomagnetic Disturbances on the Bulk Power System," North American Electric Reliability Corporation (NERC), Tech. Rep., Feb 2012.

[2] L. Marti, "Introduction to GMD Studies a Planner's Summary Roadmap for GMD Planning Studies," North American Electric Reliability Corporation (NERC), Tech. Rep., Dec 2015.

[3] "Application Guide: Computing Geomagnetically-Induced Current in the Bulk-Power System," North American Electric Reliability Corporation (NERC), Tech. Rep., Dec 2013.

[4] "Magnetotelluric Array." [Online]. Available: http://www.usarray.org/

[5] "IEEE Guide for Establishing Power Transformer Capability while under Geomagnetic Disturbances," *IEEE Std C57.163-2015*, pp. 1–50, Oct 2015.

[6] "UIUC 150-bus system." [Online]. Available: https://electricgrids.engr.tamu.edu/electric-grid-test-cases/uiuc-150-bus-system/

[7] C. Klauber, G. P. Juvekar, K. Davis, T. Overbye, and K. Shetye, "The Potential for a GIC-inclusive State Estimator," in *2018 North American Power Symposium (NAPS)*, Sep. 2018, pp. 1–6.

[8] R. Horton, D. Boteler, T. J. Overbye, R. Pirjola, and R. C. Dugan, "A test case for the calculation of geomagnetically induced currents," *IEEE Transactions on Power Delivery*, vol. 27, no. 4, pp. 2368–2373, Oct 2012.

[9] "High-Impact, Low-Frequency Event Risk to the North American Bulk Power System," North American Electric Reliability Corporation (NERC), Tech. Rep., June 2009.

[10] J. Kappenman, "A Perfect Storm of Planetary Proportions," *IEEE Spectrum*, vol. 49, no. 2, 2012.

[11] "March 13, 1989 Geomagnetic Disturbance," *1989 System Disturbances*, pp. 36–55, Aug 1990.

[12] "Transmission System Planned Performance for Geomagnetic Disturbance Events NERC Std. TPL-007-1," North American Electric Reliability Corporation (NERC), Tech. Rep., June 2014.

[13] "Transmission System Planned Performance for Geomagnetic Disturbance Events NERC Std. TPL-007-2," North American Electric Reliability Corporation (NERC), Tech. Rep., October 2017.

[14] M. Kazerooni, H. Zhu, K. Shetye, and T. J. Overbye, "Estimation of Geoelectric Field for Validating Geomagnetic Disturbance Modeling," in *Power and Energy Conference at Illinois (PECI), 2013 IEEE*. IEEE, 2013, pp. 218–224.

[15] M. Kazerooni, H. Zhu, and T. J. Overbye, "Probabilistic Modeling and Reliability Analysis for Validating Geomagnetically Induced Current Data," in *North American Power Symposium (NAPS), 2013*. IEEE, 2013, pp. 1–6.

[16] T. J. Overbye, T. R. Hutchins, K. Shetye, J. Weber, and S. Dahman, "Integration of Geomagnetic Disturbance Modeling into the Power Flow: A Methodology for Large-Scale System Studies," in *North American Power Symposium (NAPS), 2012*. IEEE, 2012, pp. 1–7.

[17] A. A. Trichtchenko, D. H. Boteler, and A. Foss, "GIC Modelling for an Overdetermined System," in *Canadian Conference on Electrical and Computer Engineering, 2006. CCECE'06.* IEEE, 2006, pp. 394–397.

[18] D. Boteler and R. Pirjola, "Comparison of Methods for Modelling Geomagnetically Induced Currents," in *Annales Geophysicae*, vol. 32, no. 9. Copernicus GmbH, 2014, pp. 1177–1187.

[19] H. Zhu and T. Overbye, "Blocking Device Placement for Mitigating the Effects of Geomagnetically Induced Currents," in *2016 IEEE Power and Energy Society General Meeting (PESGM)*, July 2016, pp. 1–1.

[20] B. Kovan and F. De Leon, "Mitigation of Geomagnetically Induced Currents by Neutral Switching," *IEEE Transactions on Power Delivery*, vol. 30, no. 4, pp. 1999–2006, 2015.

[21] M. Kazerooni, H. Zhu, T. J. Overbye, and D. A. Wojtczak, "Transmission System Geomagnetically Induced Current Model Validation," *IEEE Transactions on Power Systems*, vol. 32, no. 3, pp. 2183–2192, 2017.

[22] "ECEN615 Fall 2018-Lecture 18 by Prof. Thomas Overbye." [Online]. Available: http://overbye.engr.tamu.edu/wp-content/uploads/sites/146/2018/11/ECEN615_Fall2018_Lect18.pdf

[23] J. G. Kappenman, "An Overview of the Impulsive Geomagnetic Field Disturbances and Power Grid Impacts Associated with the Violent Sun-Earth Connection Events of 29–31 October 2003 and a Comparative Evaluation with other Contemporary Storms," *Space Weather*, vol. 3, no. 8, 2005.

[24] P. Czech, S. Chano, H. Huynh, and A. Dutil, "The Hydro-Quebec System Blackout of 13 March 1989: System Response to Geomagnetic Disturbance," in *Proc. EPRI Conf. Geomagnetically Induced Currents*, 1992.

[25] "Earth's magnetic field." [Online]. Available: https://web.ua.es/docivis/magnet/earths_magnetic_field2.html

[26] L. R. Bonner and A. Schultz, "Rapid Prediction of Electric Fields Associated with Geomagnetically Induced Currents in the Presence of three-dimensional Ground Structure: Projection of Remote Magnetic Observatory Data through Magnetotelluric Impedance Tensors," *Space Weather*, vol. 15, no. 1, pp. 204–227, 2017.

[27] "Station K and A indices." [Online]. Available: https://www.swpc.noaa.gov/products/station-k-and-indices

[28] V. D. Albertson and J. A. Van Baelen, "Electric and Magnetic Fields at the Earth's Surface due to Auroral Currents," *IEEE Transactions on Power Apparatus and Systems*, no. 4, pp. 578–584, 1970.

[29] D. Boteler, "Geomagnetically Induced Currents: Present Knowledge and Future Research," *IEEE Transactions on Power Delivery*, vol. 9, no. 1, pp. 50–58, 1994.

[30] "Regional Conductivity Maps." [Online]. Available: https://geomag.usgs.gov/conductivity/

[31] A. Schultz, G. Egbert, A. Kelbert, T. Peery, V. Clote, and B. Fry, "Staff of the National Geoelectromagnetic Facility, and their contractors," *USArray TA Magnetotelluric Transfer Functions*, 2006.

[32] A. Kelbert, G. Egbert, and A. Schultz, "IRIS DMC data services products: EMTF, the magnetotelluric transfer functions," 2011.

[33] "EM Transfer Function Product Query." [Online]. Available: http://ds.iris.edu/spud/emtf

[34] J. J. Love and A. Swidinsky, "Time Causal Operational Estimation of Electric Fields Induced in the Earth's Lithosphere During Magnetic Storms," *Geophysical Research Letters*, vol. 41, no. 7, pp. 2266–2274, 2014.

[35] D. H. Boteler and R. J. Pirjola, "Modelling Geomagnetically Induced Currents Produced by Realistic and Uniform Electric Fields," *IEEE Transactions on Power Delivery*, vol. 13, no. 4, pp. 1303–1308, Oct 1998.

[36] J. Kappenman, V. Albertson, and N. Mohan, "Investigation of Geomagnetically Induced Currents in the Proposed Winnipeg-Duluth-Twin Cities 500-kV Transmission Line," *NASA STI/Recon Technical Report N*, vol. 82, 1981.

[37] A. Viljanen, "Relation of Geomagnetically Induced Currents and Local Geomagnetic Variations," *IEEE Transactions on Power Delivery*, vol. 13, no. 4, pp. 1285–1290, 1998.

[38] V. D. Albertson, J. G. Kappenman, N. Mohan, and G. A. Skarbakka, "Load-Flow Studies in the Presence of Geomagnetically-Induced Currents," *IEEE Transactions on Power Apparatus and Systems*, vol. PAS-100, no. 2, pp. 594–607, Feb 1981.

[39] T. J. Overbye, K. S. Shetye, T. R. Hutchins, Q. Qiu, and J. D. Weber, "Power Grid Sensitivity Analysis of Geomagnetically Induced Currents," *IEEE Transactions on Power Systems*, vol. 28, no. 4, pp. 4821–4828, Nov 2013.

[40] X. Dong, Y. Liu, and J. G. Kappenman, "Comparative Analysis of Exciting Current Harmonics and Reactive Power Consumption from GIC Saturated Transformers," in *2001 IEEE Power Engineering Society Winter Meeting. Conference Proceedings (Cat. No. 01CH37194)*, vol. 1, Jan 2001, pp. 318–322 vol.1.

[41] A. Abur and A. Gomez, *Power System State Estimation-Theory and Implementations*. Marcel Dekker, Inc., 2004.

[42] A. Monticelli, "Electric Power System State Estimation," *Proceedings of the IEEE*, vol. 88, no. 2, pp. 262–282, Feb 2000.

[43] F. C. Schweppe, "Power System Static-State Estimation, Part III: Implementation," *IEEE Transactions on Power Apparatus and Systems*, vol. PAS-89, no. 1, pp. 130–135, Jan 1970.

[44] N. Shivakumar and A. Jain, "A Review of Power System Dynamic State Estimation Techniques," in *Power System Technology and IEEE Power India Conference, 2008. POWERCON 2008. Joint International Conference on*. IEEE, 2008, pp. 1–6.

[45] T. D. Mohanadhas, N. Sarma, and T. Mortensen, "State Estimation Performance Monitoring at ERCOT," in *Power Systems Conference (NPSC), 2016 National*. IEEE, 2016, pp. 1–6.

[46] "ECEN615 Fall 2018-Lecture 19 by Prof. Thomas Overbye." [Online]. Available: http://overbye.engr.tamu.edu/wp-content/uploads/sites/146/2018/11/ECEN615_Fall2018_Lect19.pdf

[47] A. B. Birchfield, K. M. Gegner, T. Xu, K. S. Shetye, and T. J. Overbye, "Statistical Considerations in the Creation of Realistic Synthetic Power Grids for Geomagnetic Disturbance Studies," *IEEE Transactions on Power Systems*, vol. 32, no. 2, pp. 1502–1510, March 2017.

[48] M. Kazerooni, H. Zhu, and T. J. Overbye, "Improved Modeling of Geomagnetically Induced Currents Utilizing Derivation Techniques for Substation Grounding Resistance," *IEEE Transactions on Power Delivery*, vol. 32, no. 5, pp. 2320–2328, Oct 2017.

[49] A. G. Exposito and A. Abur, "Generalized Observability Analysis and Measurement Classification," *IEEE Transactions on Power Systems*, vol. 13, no. 3, pp. 1090–1095, Aug 1998.

[50] B. Xu and A. Abur, "Observability Analysis and Measurement Placement for Systems with PMUs," in *IEEE PES Power Systems Conference and Exposition, 2004.*, Oct 2004, pp. 943–946 vol.2.

[51] R. D. Zimmerman, C. E. Murillo-Sanchez, and R. J. Thomas, "MATPOWER: Steady-State Operations, Planning, and Analysis Tools for Power Systems Research and Education," *IEEE Transactions on Power Systems*, vol. 26, no. 1, pp. 12–19, Feb 2011.